https://doi.org/10.5194/egusphere-2025-4169
Preprint. Discussion started: 18 September 2025

Impacts of the Three-dimensional Radiative Effects on Cloud Droplet Number Concentration Retrieval and Aerosol Cloud Interaction Analysis

Adeleke S. Ademakinwa[1], Zhibo Zhang[1,2], Daniel Miller[2,3], Kerry G. Meyer [3], Steven Platnick[3], Zahid H. Tushar[4], Sanjay Purushotham[4], and Jianwu Wang [4]

[1]*Department of Physics, University of Maryland, Baltimore County (UMBC), Baltimore, MD 21250, USA*
[2]*Goddard Earth Sciences Technology and Research (GESTAR) II, University of Maryland, Baltimore County, Baltimore, MD 21250, USA*
[3]*Earth Science Division, NASA Goddard Space Flight Center, Greenbelt, MD 20771, USA*
[4]*Department of Information Systems, University of Maryland, Baltimore County, Baltimore, MD 21250, USA*
Correspondence to: Adeleke S. Ademakinwa (adeleka1@umbc.edu).

https://doi.org/10.5194/egusphere-2025-4169
Preprint. Discussion started: 18 September 2025

Abstract

Cloud droplet number concentration (N_d) in warm liquid clouds play a crucial role in understanding cloud microphysical processes and the influence of aerosol–cloud interactions (ACI) on Earth's climate. N_d from satellite-retrieved cloud properties such as the cloud optical thickness (τ) and cloud droplet effective radius (r_e) can be biased due to the three-dimensional (3D) radiative transfer (RT) effects. Using Large-Eddy Simulation (LES) cloud fields and RT simulations, this study investigates how biases in cloud property retrievals caused by 3D-RT effects impact the derived N_d and subsequent ACI analyses. Our sensitivity studies confirm that the bi-spectral retrievals using the 3.7 μm channel—whose r_e retrieval is closest to cloud top—shows better agreement with N_d from our LES models, compared to results based on the 1.6 and 2.1 μm retrievals. At native LES resolution, N_d across all absorbing channels is strongly impacted by the 3D-effects, with the magnitude depending on the solar zenith angles (SZAs); on average, for high/low sun conditions N_d under 3D-RT underestimates/overestimates its 1D-RT counterpart, which indicates dominant darkening/brightening effects. At coarser satellite-like resolutions, average statistics between 1D and 3D retrievals agree better, indicating compensation between 3D and plane-parallel effects. Furthermore, the impact of 3D-effects on ACI analyses produced similar results across all spectral band pairings, with minimal disagreement between 1D and 3D at coarse spatial resolution. Together, these results indicate that 3D retrieval artifacts in bi-spectral N_d retrievals do not seem to drive uncertainties associated with radiative impact applications, resulting in reliable ACI and flux-related analyses.

https://doi.org/10.5194/egusphere-2025-4169
Preprint. Discussion started: 18 September 2025

1. Introduction

Aerosols influence Earth's radiative budget both directly by scattering and absorbing radiation and indirectly by modifying cloud properties. An increase in aerosol particles that serve as cloud condensation nuclei (CCN) in warm clouds typically leads to a decrease in cloud droplet effective radius (r_e), and an increase in the cloud droplet number concentration (N_d). This results in a more reflective cloud for a given liquid water path (LWP), known as the first aerosol indirect effect or Twomey effect (Twomey, 1974, 1977), leading to the radiative forcing from aerosol–cloud interactions (ACI), (RF_{aci}) (Bellouin et al., 2020; Forster et al., 2021). In addition to the Twomey effect, increased aerosol concentrations can cause additional cloud responses, such as changes in LWP and suppression of precipitation (Albrecht, 1989).

In most remote sensing–based studies of ACI, aerosol effects on clouds are estimated through changes in N_d. Therefore, continuous and accurate measurements of N_d at regional and global scales are essential to improve understanding of aerosol impacts on cloud microphysical and optical properties, as well as to evaluate RF_{aci}. Satellite-based remote sensing is commonly employed for such observations because alternative methods for measuring N_d are often limited or unavailable.

Operational satellite remote sensing instruments such as the Moderate-resolution Imaging Spectroradiometer (MODIS) do not directly retrieve N_d. Instead, N_d is derived from other retrieved parameters—namely, cloud optical thickness (τ) and r_e—under assumptions about cloud adiabatic growth and the constancy of N_d throughout the cloud depth (Boers et al., 2006; Grosvenor et al., 2018; Quaas et al., 2006). Such estimates of N_d derived from passive imager observations rely on the τ and r_e retrieved via the so-called bi-spectral retrieval techniques (e.g., Nakajima and King, 1990; Twomey and Cocks, 1989). The bi-spectral retrieval method

https://doi.org/10.5194/egusphere-2025-4169
Preprint. Discussion started: 18 September 2025

simultaneously retrieves τ and r_e using cloud reflectance measurements from two spectral bands. Typically, one band is selected from a non-absorbing visible or near-infrared (VNIR) spectral region (e.g., wavelength centered near 0.86 μm), which is primarily sensitive to τ, while the other is chosen from a moderately absorbing shortwave infrared (SWIR) (e.g., wavelength centered near 2.1 μm) or mid-wave infrared (MWIR) (e.g., wavelength centered near 3.7 μm) spectral region, which is more sensitive to r_e.

While bi-spectral retrievals from passive instruments like MODIS have significantly advanced our understanding of clouds, N_d derived from these retrievals may contain large errors and uncertainties. These arise from assumptions made both in the retrieval process and in the computation of N_d, which affect their applicability for aerosol–cloud interaction and other process studies (Gryspeerdt et al., 2016; McCoy et al., 2017; Quaas et al., 2020). Most operational bi-spectral retrievals rely on one-dimensional (1D) radiative transfer (RT) theory, which assumes that the atmosphere within each pixel is horizontally homogeneous (plane-parallel assumption) and that each pixel is independent of its neighbors (independent pixel assumption), primarily for computational efficiency. However, real clouds have complex 3D structures, requiring RT simulations that account for both vertical and horizontal radiation transport, known as "3D RT." This is challenging because detailed 3D cloud structures are generally unknown a priori, and even when available, 3D RT simulations are computationally expensive and not operationally feasible. The deviation of the 3D RT in reals cloud from the 1D RT theory as the backbone of operational cloud retrieval algorithm is often referred to as the 3D radiative effects. These effects can introduce substantial biases in cloud property retrievals and radiative quantities that are based on 1D RT (Marshak et al., 2006; Várnai and Marshak, 2002; Zhang et al., 2012, 2016). This paper focuses on investigating how errors due to 3D radiative effects associated with retrieved cloud properties

https://doi.org/10.5194/egusphere-2025-4169
Preprint. Discussion started: 18 September 2025

(τ and r_e) impact derived N_d statistics, and how these errors affect interpretations of the first aerosol indirect effect. Evaluating 3D effect errors on derived N_d from LES model fields can improve constraints on N_d, thereby provide better understanding of ACI and RF_{aci}.

From the perspective of results, 3D RT can cause brightening or darkening phenomena in observed cloud reflectance compared to 1D RT. Brightening occurs when cloud reflectance in 3D RT is higher than in 1D RT, while darkening occurs when clouds appear darker under 3D RT relative to 1D RT. These effects can significantly impact the retrievals of τ and r_e (Kato and Marshak, 2009; Marshak et al., 2006; Várnai and Davies, 1999; Várnai and Marshak, 2002). For example, brightening effects typically lead to overestimated τ and underestimated r_e retrievals, while the darkening effects typically result in underestimated τ and overestimated r_e when compared to 1D RT retrieved results (Marshak et al., 2006). Although several factors— such as, high variability in cloud top height, solar and view geometry, and photons leaking from optically thick to optically thin cloudy regions—potentially influences the 3D radiative effects, previous studies (e.g., Kato and Marshak, 2009; Marshak et al., 2006; Zhang et al., 2012) have shown that solar and observation geometry play a significant role in influencing both the sign and magnitude of 3D effects errors in bi-spectral retrievals of cloud properties (τ and r_e), with these errors being more pronounced in broken cloud fields.

Over the past decade, several studies related to aerosol–cloud interactions have utilized N_d estimates or the N_d–LWP relationship obtained from bi-spectral retrievals to study the impact of aerosols on clouds, evaluate RF_{aci}, and quantify related uncertainties. For example, Grosvenor et al. (2018) estimated that N_d from passive remote sensing instruments at the pixel scale have a relative uncertainty of 78 % (dominated by errors in r_e retrievals) for optically thick single layer

https://doi.org/10.5194/egusphere-2025-4169
Preprint. Discussion started: 18 September 2025

stratiform clouds. Quaas et al. (2020) reviewed the challenges and uncertainties in constraining the Twomey effect from satellite observations, suggesting that past studies have likely underestimated the sensitivity of N_d to aerosol perturbations, leading to an underestimation of the Twomey effect's radiative forcing. Arola et al. (2022) used satellite and simulated data to show that natural spatial variability and errors in bi-spectral retrievals of τ and r_e propagate into N_d and LWP estimates and can cause positive LWP adjustments to be misinterpreted as negative, often leading to an underestimation of the cooling effect of ACI. Gryspeerdt et al. (2019) utilized the relationship between N_d and LWP to constrain ACI. Their findings showed a highly nonlinear N_d–LWP relationship over global oceans, suggesting that LWP increases at lower N_d regimes and decreases at higher N_d regimes. Recent studies by Loveridge and Di Girolamo (2024) used a combination of synthetic cloud fields, RT simulations, and satellite observations to show that commonly used sampling strategies for N_d derived from bi-spectral retrievals, do not eliminate systematic biases caused by cloud heterogeneity, potentially leading to an overestimation of aerosol indirect effects in climate studies.

While previous studies have quantified uncertainties in N_d derivations, investigated cloud adjustments under varying environmental conditions, constrained the Twomey effect using satellite observations, and tested filtering strategies on retrieved N_d, few have specifically examined how errors arising from 3D radiative effects propagate into in N_d calculations and influence the estimation of the Twomey effect from satellite data. Understanding this linkage is crucial, as 3D radiative effects can introduce biases in cloud property retrievals that may significantly affect our interpretation of ACI.

https://doi.org/10.5194/egusphere-2025-4169
Preprint. Discussion started: 18 September 2025

The goal of this work is to build on previous studies by investigating how 3D radiative effects, which influence retrievals of τ and r_e, propagate into N_d derivations. We further aim to examine how these effects impact the analysis of the first aerosol indirect effect derived from such retrievals. Specifically, using our model LES fields, we seek to answer the following questions: *How do the brightening and darkening effects that impact the retrieved r_e and τ affect calculations of N_d? Does the derived N_d change significantly when different wavelength pairs are utilized in the bi-spectral retrievals used for the N_d calculations? And how do the 3D effects impact these changes? Finally, how do 3D effects impact our understanding of aerosol–cloud interaction analysis derived from bi-spectral retrievals?*

The paper's remaining structure is arranged as follows: Sect. 2 briefly describes the data and theory for the study. Results and discussions on how the 3D radiative effects influence calculations of N_d and ACI are presented in Sect. 3. The summary and conclusion are given in Sect. 4.

2. Data and Theory

2.1 Cloud Field Dataset

Since clouds in the real atmosphere are always influenced to some extent by 3D radiative effects, relying solely on observational data to understand these effects and their impacts on derived N_d is challenging. To address this challenge, many studies (e.g., Ademakinwa et al., 2024; Miller et al., 2018; Rajapakshe and Zhang, 2020; Zhang et al., 2012) have utilized synthetic cloud fields and RT simulations to mimic the satellite observation-retrieval process and study the 3D radiative effects on retrieved τ and r_e. A major advantage of this approach is that the LES cloud field provides the model "truth" which is difficult to obtain in real world observations. Also, the flexibility of this approach allows investigation of various cloud mechanisms at different levels of

https://doi.org/10.5194/egusphere-2025-4169
Preprint. Discussion started: 18 September 2025

complexity. For example, we can analyze the 3D RT impacts by comparing retrievals from 3D RT with those from 1D RT. Disadvantages of this approach are that the usefulness of such a study depends on the realism of the synthetic microphysical and water content fields; which, like the satellite retrievals themselves are difficult to validate, as well as the limited variability in scene properties that can be run and processed compared to global satellite sampling.

This study utilizes a similar state-of-the-art satellite retrieval simulator as in Zhang et al. (2012) and Ademakinwa et al. (2024) that applies 1D and 3D RT simulations to synthetic cloud fields. In this work, our cloud fields are Large Eddy Simulation (LES) models (Distributed Hydrodynamic-Aerosol-Radiation Modeling Application (DHARMA)) with bin microphysics (Ackerman et al., 2004; Miller et al., 2016; Zhang et al., 2012). These LES are representative of a trade wind cumulus regime, characterized by scattered cumulus clouds rising into a thin, broken stratocumulus layer. They consist of different initial aerosol loadings derived from an idealized case study by Stevens et al. (2001) conducted during the Atlantic Trade Wind Experiment (ATEX). Three LES cases of different initial aerosol loadings are examined throughout this study. The first case has a CCN loading of 40 cm^{-3} (hereafter referred to as "ATEX clean"), the second case has a CCN loading of 75 cm^{-3} (hereafter referred to as "ATEX control"), while the third case has a CCN loading of 600 cm^{-3} (hereafter referred to as "ATEX polluted"). The LES provides a model "truth" for the 3D cloud microphysical properties, which are used as a baseline for comparisons with numerically simulated retrievals. The droplet sizes in the LES consist of 25 bins used to represent the distribution of droplet sizes (Ackerman et al., 1995) and Mie scattering properties are bulk averaged over a highly resolved flat sub-bin to obtain the optical properties for each size bin. This serves as input for RT simulations based on the size distributions of the LES cloud fields. The LES cases have a domain size of $9.6 \times 9.6 \times 3$ km ($x \times y \times z$), with a horizontal spatial

https://doi.org/10.5194/egusphere-2025-4169
Preprint. Discussion started: 18 September 2025

resolution of $\Delta x = \Delta y = 100$ m and a constant vertical grid spacing of $\Delta z = 40$ m. These grid resolutions were selected such that individual cumulus clouds are appropriately resolved; however, it is expected to exhibit vertical artifacts near the inversion due to unresolved entrainment processes at these resolutions (Stevens et al., 2002). Additional information about the model setup for these LES cases can be found in Fridlind and Ackerman (2011) and Zhang et al. (2012). For each LES case, snapshots of cloud microphysical properties are taken every half hour after the first 4 hours of each simulation, resulting in 9 cloud scenes per LES case and a total of 24 cloud fields.

The LES cloud fields comprise of spatially inhomogeneous microphysical properties, and these cloud properties change as the LES cloud field evolves at each time step. Figure 1 provides a map of the τ derived from the LES droplet size distributions for the ATEX clean, control and polluted cases at 4.0 hours of simulation time. The map shows that the scenes are typically characterized by broken clouds with cloud fraction (CF; defined as a fraction of columns with $\tau >$ 0.3) greater than 70 % in each LES case (CF of 73.7, 77. 2 and 73.3 % for the ATEX clean, control and polluted cases respectively).

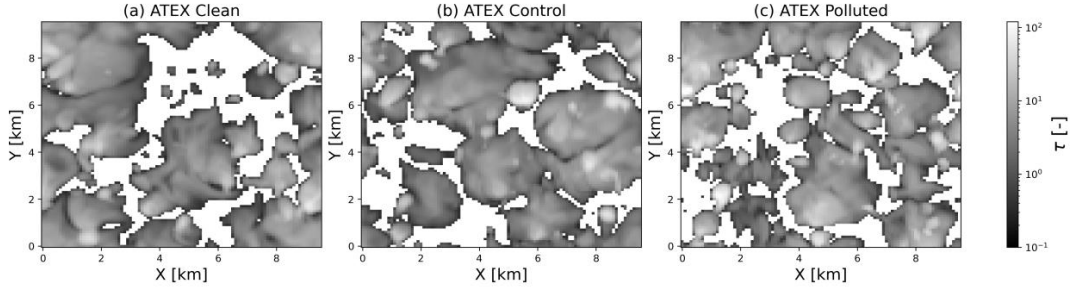

Figure 1. Map of the Large Eddy Simulation (LES) cloud optical thickness (τ) for the (a) ATEX clean, (b) ATEX control, and (c) ATEX polluted case at the 4 h simulation time.

https://doi.org/10.5194/egusphere-2025-4169
Preprint. Discussion started: 18 September 2025

2.2. Radiative Transfer Setup

The spherical harmonics discrete ordinate method (SHDOM) RT model developed by Evans (1998) was utilized to model reflectance for both 3D and 1D RT at the native LES resolution of 100 m. The RT simulations were performed for 6 solar zenith angles (SZAs) spanning from 10° to 60° in increments of 10°. A fixed nadir viewing zenith angle (VZA), and a constant relative azimuthal angle ($\Delta\Phi$= 30°) were used throughout the study. The simulations for cloud retrievals are performed based on MODIS spectral response function for MODIS Band 2 (0.86 μm), Band 6 (1.6 μm), Band 7 (2.1 μm), and Band 20 (3.7 μm). We hereafter refer to these bands by their respective nominal wavelengths. It is important to note that although the 3.7 μm channel normally comprise of both solar and thermal portion and recent study by Loveridge and Di Girolamo (2024) suggest that contribution of the thermal emission to the error budget in the 3.7 μm retrieved r_e can sometimes be significant—partly due to their analysis utilizing partly cloudy pixels. This work assumes that the thermal emission in the 3.7 μm band can be removed with no error and thus have used only the solar portion in our RT calculations. For all RT simulations in this study, the surface was assumed to be Lambertian with an albedo of 5 % (an assumption approximating ocean surfaces under diffuse illumination), and double periodic horizontal boundary conditions were applied.

Observational studies usually estimate cloud susceptibility from derived N_d and broadband flux observations from Clouds and the Earth's Radiant Energy System (CERES) (e.g Painemal and Minnis 2012; Platnick and Oreopoulos 2008). In our previous study (Ademakinwa et al. 2024), we have developed a framework to simulate the broadband flux from LES simulations using the combination of 3D radiative transfer model (SHDOM and I3RC) a correlated k-distribution (CKD) model. It is important to note that the broadband flux simulated by the 3D RT model (F_{3D}) is fundamentally different from that estimated by CERES algorithm (F_{BB}^{CERES}). In particular, the

https://doi.org/10.5194/egusphere-2025-4169
Preprint. Discussion started: 18 September 2025

pixel-to-pixel variation of F_{3D} is much smaller than F_{BB}^{CERES} because the F_{3D} is computed at the top of the domain based on the radiances coming from different pixels leading to a spatial-averaging effect. In contrast, F_{BB}^{CERES} is estimated based on the directional broadband radiance ($I_{BB}(\Omega)$) and angular distribution model ($ADM(\Omega)$), where Ω represents the full scattering geometry. From these observations and the ADM, flux is obtained by the following, $F_{BB}^{CERES} = I_{BB}(\Omega)/ADM(\Omega)$. While $I_{BB}(\Omega)$ varies from pixel to pixel, $ADM(\Omega)$ is scene context dependent and does not vary for a small LES domain. Because of the absence of spatial averaging (coarse resolution), the pixel-to-pixel variation of F_{BB}^{CERES} is significantly larger than F_{3D}— due to radiative smoothing at small scales. The difference between modeled F_{3D} and F_{BB}^{CERES} is beyond the scope of this study.

Because the pixel-to-pixel variation is critical for the derivation of cloud susceptibility, we adopt the CERES-like F_{BB}^{CERES} in this study. Furthermore, because the ADM is the same for all the cloudy pixels, the spatial variation of F_{BB}^{CERES} is determined by $I_{BB}(\Omega)$. Therefore, in this study we simply use the simulated broadband reflectance $R(\Omega) = \pi I_{BB}(\Omega)/(\mu_0 F_0)$ to derive the cloud susceptibility (μ_0 is the cosine of SZA and F_0 is the top of medium solar flux). To that end, we focus here on relative deviations of nadir-viewing broadband reflectance (R_{BB}) rather than albedo in the calculation of susceptibility. We expect that deviations between 1D and 3D reflectance will be proportional to calculations based on broadband reflected fluxes and scene albedo. The modeled nadir-viewing broadband shortwave (0.3 – 5 μm) reflectance are calculated for 13 out of the 14 Rapid Radiative Transfer Model (RRTM) spectral bands in the shortwave. Notably, we have excluded RRTM band 28 (0.2 - 0.26 μm) from these calculations because our Mie property computations failed for large droplet size bins (large size parameter). This exclusion is unlikely to impact the results significantly because this band contributes very little to the solar shortwave radiative energy budget.

https://doi.org/10.5194/egusphere-2025-4169
Preprint. Discussion started: 18 September 2025

2.3. Bi-Spectral Retrieval Method

The bi-spectral retrieval method described in Sect. 1 was applied to the simulated reflectance (see Sect. 2.3 in Ademakinwa et al., 2024). This method relies exclusively on homogeneous 1D RT assumptions to interpret the observed cloud reflectance. Its implementation is done using a precomputed lookup table (LUT), which includes computed 1D spectral reflectance for different τ and r_e combinations and solar-view geometries. The LUT then is used to find the τ and r_e whose computed reflectance best matches the observed (here, modeled LES) cloud reflectance. Notably, for small τ, retrieval uncertainty increases because the isolines of the LUT are less orthogonal and more tightly packed. This LUT non-orthogonality has significant consequences for observations with high spatial inhomogeneity below the pixel level resolution (Zhang et al., 2012, 2016) leading to the plane parallel homogeneous approximation (PPHA) bias. The consequences of both unresolved inhomogeneity and 3D radiative effects changes with spatial resolution and are examined in Sect. 3.3.

The VNIR reflectances used for the bi-spectral retrievals were calculated for 0.86 µm, while the SWIR and MWIR reflectances were calculate for the 1.6, 2.1 and 3.7 µm channel. We use a simplified cloud masking method that makes use of the 0.86 µm reflectance (i.e., R (0.86 µm) > 0.07) to identify cloudy pixels after radiative transfer simulations. The LUTs for this study have 73 effective radii spanning from 4 to 40 µm and 105 log-spaced τ values spanning from 0.1 to 150. A constant effective variance (v_e) value of 0.1 in the gamma representation of the droplet size distribution is applied, consistent with operational MODIS retrievals. For consistency, the same surface albedo of 5 % used in all our LES RT reflectance simulations is applied in the LUT reflectance simulations.

https://doi.org/10.5194/egusphere-2025-4169
Preprint. Discussion started: 18 September 2025

We implement retrievals using reflectance simulations at the native LES resolution (100 m) and spatially average to a coarser MODIS-like resolution. For the MODIS-like resolution retrievals, we averaged reflectance from the LES resolution of 100 m to 800 m resolution and utilized this area-averaged reflectance as input into the LUT for retrievals. Note that we have used 800 m resolution instead of the MODIS nadir 1 km because it divides evenly into our LES domain. Also, sensitivity analyses (not presented) suggest minimal differences between τ and r_e retrievals at 800 m and 1 km resolutions.

When averaging from high resolution to coarse resolution, we distinguish between overcast and partially cloudy pixels, depending on whether or not clear-sky pixels are included in the average reflectance. Firstly, if one or more pixels used for the area average is a clear-sky pixel, we classify the resulting pixel as a "partially cloudy pixel". Secondly, if all pixels utilized for the area average are cloudy, we classify the averaged resulting pixel as an "overcast cloudy pixel". With this, we define a category "all cloudy pixels" to consist of both partially cloudy and overcast cloudy pixels.

Cloud property retrievals that utilize area-averaged reflectances are impacted by unresolved (i.e., sub-pixel) spatial cloud inhomogeneity that can bias retrieval results, especially if the average is done over a highly inhomogeneous τ region. For example, Zhang et al. (2012) demonstrated using RT simulations how the nonlinearity in the LUT space (non-orthogonality of the τ and r_e LUT grid) can lead to plane-parallel albedo bias (Cahalan et al., 1994; the retrieved τ from the average reflectance of inhomogeneous cloud pixels tends to be smaller than the average of the sub-pixel τ) and plane-parallel r_e bias (r_e retrieved from area-averaged reflectances over inhomogeneous τ region is overestimated compared the original r_e).

https://doi.org/10.5194/egusphere-2025-4169
Preprint. Discussion started: 18 September 2025

2.4. N_d and LWP Estimates

2.4.1. N_d and LWP from LES

Cloud vertical structures in realistic cloud fields, such as the LES cases considered in this study, have microphysical properties (e.g., N_d and LWC) that vary vertically within each profile. Therefore, describing a single representative microphysical property value as a reference in the LES, requires accounting for the vertical distribution of the profile and on the application of interest. For example, the reference N_d for in situ studies is typically taken as an average value of N_d across the cloud vertical extent, from the cloud base height (CBH) to the cloud top height (CTH). Because our study aims to compare remote sensing retrievals of N_d, we define our reference in such a way that is radiatively representative of the cloud layer. Thus, we weight N_d over the extinction coefficient (β_{ext}) at each layer (z) as given by:

$$N_{d\_LES} = \frac{1}{\tau}\int_{CTH}^{CBH} N_d(z)\,\beta_{ext}(z)\,dz. \quad (1)$$

With this definition, layers with higher β_{ext} contribute more to the weighted value because they play a larger role in how the cloud interacts with scattered radiation. Also, the column LWP from the LES (LWP_{LES}) is obtained by integrating vertically the cloud liquid water content (LWC) from CBH to CTH in each column, expressed as:

$$LWP_{LES} = \int_{CTH}^{CBH} LWC(z)dz. \quad (2)$$

https://doi.org/10.5194/egusphere-2025-4169
Preprint. Discussion started: 18 September 2025

2.4.2. Satellite-Based N_d and LWP Retrievals

Following previous studies, we calculate N_d from bi-spectral retrievals of τ and r_e following a pseudo-adiabatic model which assumes that (i) the LWC increases linearly (as a fixed fraction of its adiabatic value) with the cloud geometrical height and that (ii) N_d is constant vertically. Here, N_d is obtained from τ and r_e (denoted as N_{d_cal}) according to Grosvenor et al. (2018):

$$N_{d\_cal} = \frac{\sqrt{5}}{2k\pi}\left(\frac{f_{ad} c_w \tau}{Q_{ext}\rho_w\, r_e^5}\right)^{1/2} \quad (3)$$

where f_{ad} is the pseudo-adiabatic factor (constrained between 0 and 1), c_w is the effective condensation rate ($g\ m^{-4}$), Q_{ext} is the bulk extinction efficiency derived from Mie theory (approximated as 2 in the geometric scattering limit), and ρ_w is the density of liquid water (taken as $1\ g\ cm^{-3}$) and the parameter k is defined as:

$$k = \left(\frac{r_v}{r_e}\right)^3 \quad (4)$$

where r_v is the droplet mean volume radius. Several values of k have been applied in N_d related studies and in operational remote-sensing that derive N_d from τ and r_e retrieved by the bi-spectral method. For example, the MODIS N_d calculation assume a constant value of k = 0.72 (Grosvenor et al., 2018). Brenguier et al. (2011) utilized in situ measurements collected during five distinct field experiments to show that k values vary between 0.7 and 0.9, with uncertainties ranging from 10 % to 14 % across different cloud types and atmospheric conditions. Loveridge and Di Girolamo (2024) applied a k value obtained from domain-average of their stochastically generated cloud

https://doi.org/10.5194/egusphere-2025-4169
Preprint. Discussion started: 18 September 2025

fields in deriving N_d. All these suggests different values of k depending on the cloud regime. Studies based on in situ measurements have shown that k can vary significantly (Martin et al., 1994) and may also change under particularly extreme aerosol conditions (Noone et al., 2000). Thus, if k is not properly represented, it can introduce significant uncertainty into the calculation of N_d. To avoid these unconstrained constants driving our understanding of retrieval behavior, throughout this work we have calculated both k, and the quasi-adiabatic lapse rate ($f_{ad}c_w$) in each cloudy column directly from the LES cloud field.

Several studies that derive N_d from bi-spectral retrieved cloud properties commonly utilize filtering techniques based on several criteria to minimize uncertainties in N_d estimates, which arise from from errors in retrieving r_e and τ from the bi-spectral method, especially in highly variable cloud fields (Grosvenor et al., 2018; Gryspeerdt et al., 2022; Loveridge and Di Girolamo, 2024; Quaas et al., 2006). However, this filtering methodology can unintentionally exclude certain types of clouds, limiting the analysis to specific cloud regimes. To avoid this bias, and to effectively quantify all possible sources of uncertainty, we incorporate all available N_d data without applying any pre-filtering method beyond the cloud mask. Furthermore, prior filtering schemes (e.g., Gryspeerdt et al., 2022; Zhu et al., 2018) implemented for coarser-resolution satellite observations may not be appropriate for the native LES resolution (100 m). For analysis involving LWP, we obtain the derived LWP (LWP_{cal}) from the retrieved τ and r_e by the adiabatic relationship given as (Wood and Hartmann 2006):

$$LWP_{cal} = \frac{5}{9}\rho_w r_e \tau \tag{5}$$

https://doi.org/10.5194/egusphere-2025-4169
Preprint. Discussion started: 18 September 2025

3. Results and discussion

3.1. LES N_d and Derived N_d Comparisons

We first perform a RT closure comparison between the reference N_d obtained directly from the LES (N_{d_LES}) and the N_d derived from Eq. (3) using τ and r_e retrieved from homogeneous plane parallel RT-based simulated reflectance from the 0.86 μm channel paired with an absorbing wavelength channel λ_{abs}, ($N_{d\_cal}^{1D}(\lambda_{abs})$). This closure comparison allows us to (i) check the methodology of our retrieval algorithm and (ii) investigate N_d errors associated with adiabatic cloud model assumptions. Figure 2 shows these comparisons as a regression plot of $N_{d\_cal}^{1D}(\lambda_{abs})$ vs. N_{d_LES} for the ATEX clean, control and polluted cases at 4.0 hours of simulation time, when λ_{abs} is 1.6, 2.1 and 3.7 μm. The comparison shows a general good agreement between $N_{d\_cal}^{1D}(\lambda_{abs})$ and N_{d_LES} for the ATEX clean, ATEX control and to some extent the ATEX polluted case with correlation coefficient (R) of 0.847, 0.852 and 0.748, respectively, when λ_{abs} is 1.6 μm; 0.885, 0.867 and 0.748 when λ_{abs} is 2.1 μm; and 0.859, 0.856 and 0.790 when λ_{abs} is 3.7 μm. The disparities observed in this comparison indicate that deviations from adiabatic conditions are common in the LES simulations, which can bias the derived N_d. Furthermore, the ATEX polluted case appears to deviate the most from the adiabatic assumption.

https://doi.org/10.5194/egusphere-2025-4169
Preprint. Discussion started: 18 September 2025

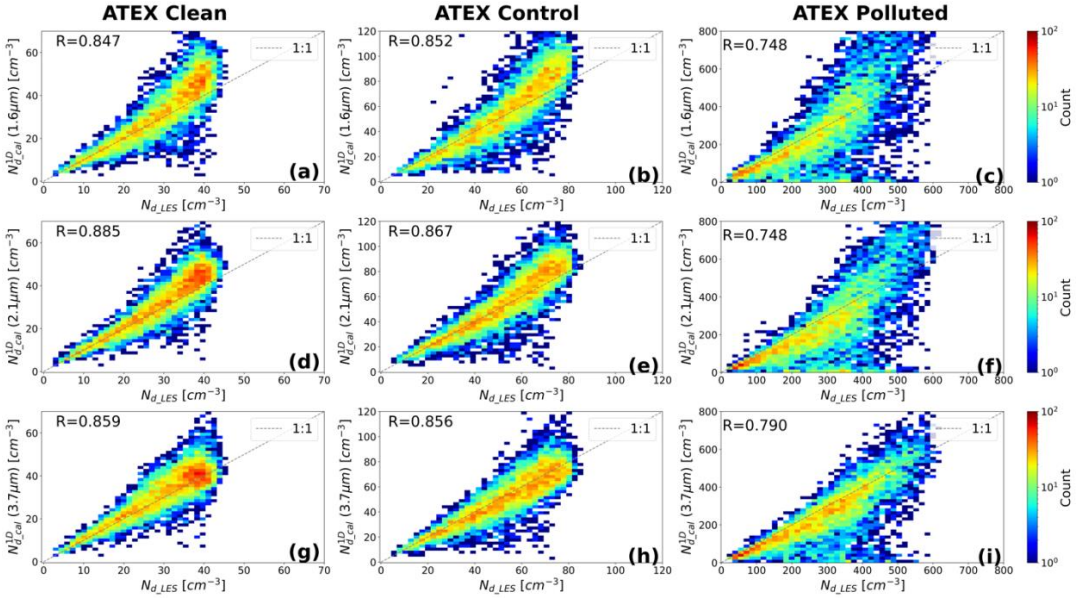

Figure 2. Comparison of N_d derived from 1D RT bi−spectral retrievals ($N_{d\_cal}^{1D}(\lambda_{abs})$) versus N_d obtained from the LES (N_{d_LES}) for (a) ATEX clean, (b) ATEX control and (c) ATEX polluted for retrievals at absorbing channel, (λ_{abs}) of 1.6 μm, for (d) ATEX clean, (e) ATEX control and (f) ATEX polluted for retrievals at λ_{abs} of 2.1 μm and for (g) ATEX clean, (h) ATEX control and (i) ATEX polluted for retrievals at λ_{abs} of 3.7 μm at 4 h of simulation time. Note: 1D RT and bi−spectral retrievals utilized for this comparison were carried out at SZA 50^o. Dotted lines indicate 1:1 relationship between the derived and LES N_d.

Although some deviations occur in the 1D RT closure comparison, they still provide greater confidence in our derived N_d and in our definition of the reference N_d (for reference, Appendix A1 shows comparisons of N_d from 1D RT and N_d from the LES when defined as a vertical column average without extinction weighting). Establishing the underlying physical processes influencing the N_d estimates obtained from the LES and retrievals are challenging when relying solely on direct one-to-one comparison. Instead, we evaluate the probability density functions (PDFs) of N_{d_LES} against those obtained from the derived N_d . For the PDF comparison, data across all time steps within each LES case are combined to ensure robust statistical analysis. Apart from evaluating the PDFs of N_{d_LES} and $N_{d\_cal}^{1D}(\lambda_{abs})$, we also investigate errors associated with the adiabatic cloud model assumptions in Eq. (3). This is done by introducing constraints on

https://doi.org/10.5194/egusphere-2025-4169
Preprint. Discussion started: 18 September 2025

the retrieved r_e and τ used to compute N_d, which increasingly force conformity with the level of adiabaticity in the LES itself. First, we utilize the vertically weighted (VW) r_e (denoted as r_e(VW)), computed using the relationship defined by Miller et al. (2016) (check their Eq. (14)), and optical thickness (τ_{tot}) from the LES into Eq. (3) to derive N_d (denoted as $N_{d\_cal}^{r_e(VW),\tau_{tot}}$). Second, we use droplet effective radius of the layer where the LWC is maximum as a representative of the adiabatic cloud top r_e (denoted as r_e^*) and τ_{tot} as inputs in Eq. (3) to derive N_d (denoted as $N_{d\_cal}^{r_e^*,\tau_{tot}}$). Last, we derive N_d, by using r_e^* and cloud optical depth computed from the LES that excludes cloud optical depth contributions from drizzle drops sizes (r) by isolating $r > 30\ \mu m$ from the droplet size distribution (denoted as $\tau_{no\ drizzle}$). N_d obtained from this r_e^* and $\tau_{no\ drizzle}$ is denoted as $N_{d\_cal}^{r_e^*,\tau_{no\ drizzle}}$. The idea of testing with r_e^* is because it is representative of the droplet radius profile that follows the adiabatic assumption of the retrieval — absent significant entrainment modification at cloud top or model resolution artifacts. PDFs of N_d obtained from the LES, those inferred from the retrievals under 1D RT (at SZA 50°) when λ_{abs} is $1.6,\ 2.1\ and\ 3.7\ \mu m$, and those derived from retrievals under the different levels of constraints earlier discussed, for the ATEX clean, ATEX control, and ATEX polluted cases are presented in Figure 3. In the ATEX clean and control cases (Figure 3a and b), the N_{d_LES} distributions peak around their respective aerosol loading values (i.e., peak around 40 cm^{-3} and 75 cm^{-3} for the ATEX clean and control cases respectively). This indicates that most of the available CCN are activated into cloud droplets. On the other hand, the lower values of the N_{d_LES} observed in the distribution are attributed to increased collision-coalescence as well as N_d removal processes driven by entrainment and precipitation.

https://doi.org/10.5194/egusphere-2025-4169
Preprint. Discussion started: 18 September 2025

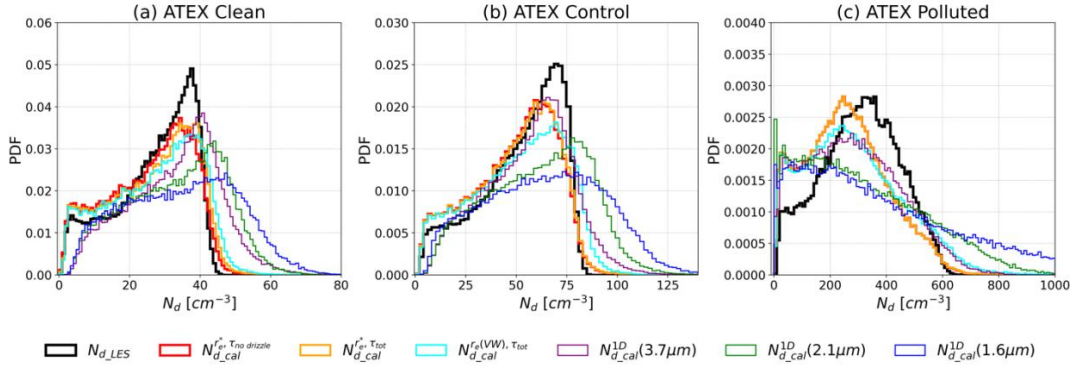

Figure 3. Probability Density Functions (PDFs) of N_d obtained from the LES ($N_{d\ LES}$) and N_d calculated from the adiabatic equation using 1D RT derived cloud properties (for absorbing channels 1.6 μm, 2.1 μm and 3.7 μm), and under different levels of controls across all time steps for the ATEX clean, control and polluted cases in (a), (b) and (c) respectively. Note the $N_{d\_cal}^{r_e^*,\tau\ no\ drizzle}$ PDF is being covered by the $N_{d\_ret}^{r_e^*,\tau\ tot}$ PDF in the ATEX control and polluted cases because drizzle is significantly minimal and not driving any vertical profile changes.

Interestingly, the PDF distribution of N_{d_LES} for the ATEX polluted case (black line in Figure 3c) is somewhat different from those of the clean and control cases. Its PDF has a peak around 300 cm^{-3}, which is significantly less than the initial aerosol loading value (CCN 600 cm^{-3}). This is probably because not all the CCNs are activated in the ATEX polluted case. When we consider the PDF of the $N_{d\_cal}^{1D}(\lambda_{abs})$ (for the three absorbing channels considered in this study) for the ATEX clean and control cases, similar cloud processes to the N_{d_LES} are observed, but with PDFs having a broader range and higher N_d peak values, and notably long tails towards larger values, indicating overestimation. The N_d overestimation statistics is more pronounced in $N_{d\_cal}^{1D}(1.6\mu m)$, reduces for $N_{d\_cal}^{1D}(2.1\mu m)$ and is smallest for $N_{d\_cal}^{1D}(3.7\mu m)$. This suggests that $N_{d\_cal}^{1D}(3.7\mu m)$ agrees the most with N_{d_LES} compared to results from the other two absorbing channels. When we consider the $N_{d\_cal}^{1D}(\lambda_{abs})$ PDFs from the ATEX polluted case (blue, green and purple lines in Figure 3c), the peaks for all three absorbing channels are at smaller values than that of the N_{d_LES}, although all have long tails towards larger values indicating significant

https://doi.org/10.5194/egusphere-2025-4169
Preprint. Discussion started: 18 September 2025

417 overestimation remains. For the ATEX polluted case, the $N_{d\_cal}^{1D}(3.7\mu m)$ PDF still has the smallest
418 overestimation compared to the $N_{d\_cal}^{1D}(1.6\mu m)$ and $N_{d\_cal}^{1D}(2.1\mu m)$ results.

419 In general, the disparity in $N_{d\_cal}^{1D}(\lambda_{abs})$ obtained for all λ_{abs} (1.6, 2.1 and 3.7 μm) is due
420 primarily to differences in the retrieved r_e—in vertically inhomogeneous clouds, satellite-based
421 r_e retrievals via the bi-spectral method can vary for different channels due to spectrally-varying
422 liquid water absorption (Meyer et al., 2025) leading to different penetration depths within a cloud
423 (Platnick, 2000). The 3.7 μm being the most absorptive and 1.6 μm being the least absorptive of
424 the three channels. For ideal clouds, the 3.7 µm channel is most absorptive and yield r_e retrievals
425 closer to the cloud top compared to the less absorbing 2.1 µm channel, and the 1.6 µm channel is
426 the least absorptive and yields retrievals deepest into the cloud. Since the N_d equation (Eq. (3)) is
427 most sensitive to r_e (r_e has the largest exponent in Eq. (3); $N_{d\_cal}\, \alpha\, r_e^{-5/2}$), small changes in r_e
428 will greatly impact the derived N_d. Thus, the reasonable agreement observed between the PDF of
429 $N_{d\_cal}^{1D}(3.7\mu m)$ and N_{d_LES} is not surprising since Eq. (3) assumes r_e is at cloud top. This is
430 corroborated by previous studies (e.g., Zhang and Platnick, 2011) that indicate that in adiabatic
431 clouds, the 3.7 µm r_e retrieval is expected to be larger than retrievals from shorter wavelengths
432 (and 2.1 µm r_e retrieval > 1.6 µm r_e retrieval), although this relationship can be affected by other
433 factors including retrieval biases.

434 In general, the $N_{d\_cal}^{1D}(\lambda_{abs})$ results in Figure 3 from the three absorbing channels indicate
435 that, even when the RT makes the same plane-parallel assumptions as the retrievals, there are
436 notable variabilities in the derived $N_{d\_cal}^{1D}(\lambda_{abs})$ when compared to N_{d_LES}. These variabilities
437 could be due to various reasons, which include inconsistencies between the vertical distribution of
438 cloud microphysics in the LES truth and the assumptions that form the basis of the N_d equation

https://doi.org/10.5194/egusphere-2025-4169
Preprint. Discussion started: 18 September 2025

utilized for the retrievals. Recall, the N_d derived from Eq. (3) assumes that the cloud is adiabatic i.e., LWC increases monotonically with height from cloud base to cloud top and N_d is constant vertically. But not all columns in the LES are adiabatic. Various processes such as entrainment, coalescence, etc. which are prevalent in natural clouds (and evident in this study LES cloud fields) introduce sub- or super-adiabatic behaviors in cloud vertical profiles, which impacts derived N_d. When we consider the PDF of calculated N_d when τ and r_e are constrained to various degrees using values derived directly from the LES cloud field, one would expect the $N_{d\_cal}^{r_e(VW),\tau\ tot}$ to agree the most with the reference N_{d_LES}, since $r_e(VW)$ and τ_{tot} are from the LES. But this is not the case, as the $N_{d\_cal}^{r_e(VW),\tau\ tot}$ PDF shows substantial deviations from the PDF of N_{d_LES}. A reason for this is that $r_e(VW)$ represents a weighted vertical average which is highly sensitive to the cloud microphysics and vertical structure of r_e, especially if the optical extinction in the cloud entrainment region is large enough to impact the $r_e(VW)$. The PDF of $N_{d\_cal}^{r_e^*,\tau\ no\ drizzle}$ which is derived from the most adiabatic governed τ and r_e, shows the most agreement with the N_{d_LES} for all LES cases. On the other hand, the derived PDF's agreement with N_{d_LES} reduces as the adiabatic realism of the input properties decreases; $N_{d\_cal}^{r_e^*,\tau\ tot}$ showing better agreement with N_{d_LES} than $N_{d\_cal}^{r_e(VW),\tau\ tot}$ and N_{d_LES} comparison.

It is important to note that the PDFs of $N_{d\_cal}^{r_e^*,\tau\ no\ drizzle}$ and $N_{d\_cal}^{r_e^*,\tau\ tot}$ are very similar in the ATEX control and polluted cases as neither forms significant drizzle that can cause vertical profile changes.

https://doi.org/10.5194/egusphere-2025-4169
Preprint. Discussion started: 18 September 2025

3.2. Impact of 3D Radiative Effects on Derived N_d at the Native LES Resolution

To investigate the 3D radiative effects impacts on the derived N_d, we compare $N_{d\_cal}^{1D}(\lambda_{abs})$ with N_d derived from Eq. (3) using τ and r_e retrieved from 3D RT-based simulated reflectance at λ_{abs} ($N_{d\_cal}^{3D}(\lambda_{abs})$). We carry out this comparison at different SZAs, ranging from high to low sun positions. Figure 4 shows the PDF of $N_{d\_cal}^{1D}(\lambda_{abs})$ and $N_{d\_cal}^{3D}(\lambda_{abs})$ derived at the LES resolution (100 m) for a high sun (SZA 10^o), moderate sun (SZA 30^o) and a more oblique sun position (SZA 50^o) across all time steps (combined) in each of the ATEX clean, control and polluted LES cases.

When the sun is high, the PDFs of $N_{d\_cal}^{1D}(2.1\mu m)$ is almost similar to those of $N_{d\_cal}^{3D}(2.1\mu m)$ (black line in Figures 4a, d and g). Some level of similarity is also observed for the $N_{d\_cal}^{1D}(\lambda_{abs})$ and $N_{d\_cal}^{3D}(\lambda_{abs})$ PDFs obtained when $\lambda_{abs} = 1.6$ and $3.7\ \mu m$, as they peak around similar N_d regions (although the peaks of the $N_{d\_cal}^{3D}(3.7\mu m)$ are smaller compared to $N_{d\_cal}^{1D}(3.7\mu m)$). They also exhibit similar physical cloud processes as the N_{d_LES} described in Sect. 3.1. A reason for this similarity is the minimal 3D effects (lack of extreme darkening and brightening) when the sun is high. Thus, the reflectance signal utilized for the cloud property retrieval under 3D RT at high sun is comparable to its 1D RT counterpart and yields comparable derived N_d. Results for SZA 30^o, show that the PDF of $N_{d\_cal}^{3D}(\lambda_{abs})$ broadens and a narrow peak is observed towards small $N_{d\_cal}^{3D}(\lambda_{abs})$ values (Figure 4b, e and h). This narrow peak occurs where τ is underestimated and r_e is overestimated (a result of the darkening effects).

https://doi.org/10.5194/egusphere-2025-4169
Preprint. Discussion started: 18 September 2025

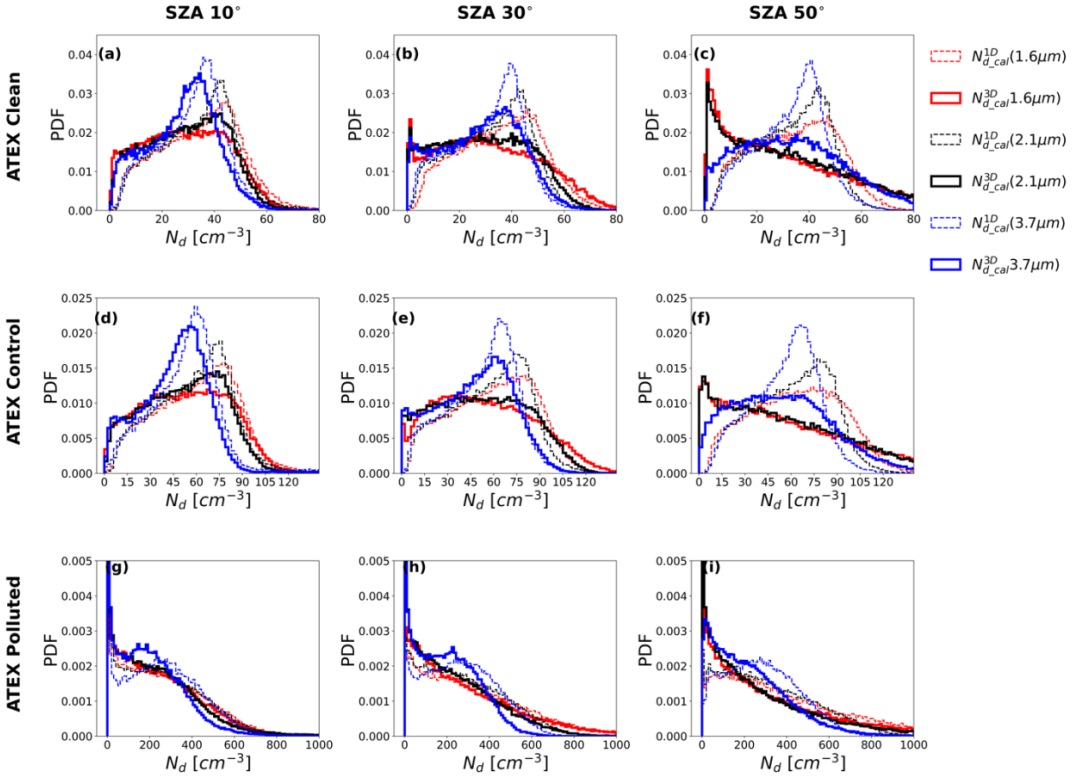

Figure 4. Probability Density Functions (PDFs) of $N^{1D}_{d\_cal}(\lambda_{abs})$ and $N^{3D}_{d\_cal}(\lambda_{abs})$ at native LES 100 m resolution at SZA 10, 30 and 50 degrees for the ATEX clean, control and polluted case at all time steps. Where λ_{abs} is the absorbing channel paired with 0.86 μm in the bi-spectral retrieval.

Also, the PDF of $N^{3D}_{d\_cal}(\lambda_{abs})$ extends to larger N_d values, compared to $N^{1D}_{d\_cal}(\lambda_{abs})$. These larger $N^{3D}_{d\_cal}(\lambda_{abs})$ values correspond to where τ is overestimated and r_e is underestimated (a result of the brightening effects). Overall, though, it appears that the shadowing effect is predominant in $N^{3D}_{d\_cal}(\lambda_{abs})$ for both high and moderate sun positions (discussed further in the domain-averaged plot in Figure 5). When the sun is low, the PDF of $N^{3D}_{d\_cal}(\lambda_{abs})$ become very broad, with larger peaks at the smallest N_d, longer tails at large N_d, and a flattening of the peaks at moderate N_d that are observed in the high and moderate sun cases. This observed pattern is due

https://doi.org/10.5194/egusphere-2025-4169
Preprint. Discussion started: 18 September 2025

to both brightening and darkening effects occurring simultaneously in the cloud property retrievals and contribute to the overestimate of $N_{d\_cal}^{3D}(\lambda_{abs})$ (brightening effect) and underestimate of $N_{d\_cal}^{3D}(\lambda_{abs})$ (darkening effect) compared to $N_{d\_cal}^{1D}(\lambda_{abs})$. To examine the overall 3D radiative effect impact on the derived N_d at the LES domain scale, we calculate the in-cloud domain average of the retrieved N_d for each LES case at the different SZA's listed in Sect. 2 (SZA= [10°: 60°] in steps of 10°). These domain-averaged $N_{d\_cal}^{3D}(\lambda_{abs})$ and $N_{d\_cal}^{1D}(\lambda_{abs})$ comparisons will provide insight on which 3D radiative effect (brightening or darkening) error is dominant (on the domain scale) in the cloud property retrievals (r_e and τ) that are utilized for the N_d calculations. Figure 5 shows the domain average of $N_{d\_cal}^{3D}(\lambda_{abs})$ and $N_{d\_cal}^{1D}(\lambda_{abs})$ at the six SZA's for the ATEX clean, control and polluted cases averaged over all time steps for λ_{abs} of 1.6, 2.1, and 3.7 μm.

https://doi.org/10.5194/egusphere-2025-4169
Preprint. Discussion started: 18 September 2025

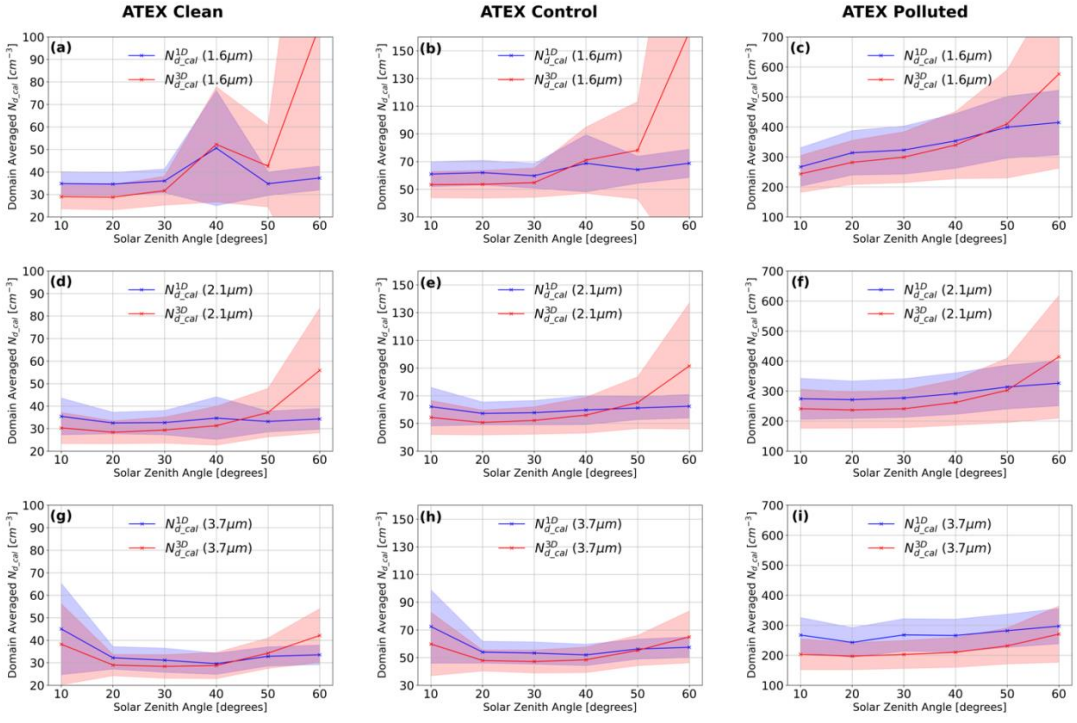

Figure 5. Domain average of $N_{d\_cal}^{1D}(\lambda_{abs})$ and $N_{d\_cal}^{3D}(\lambda_{abs})$ as a function of solar zenith angle for the ATEX clean, ATEX controlled and ATEX polluted case averaged across all time steps for λ_{abs} = 1.6, 2.1, and 3.7 μm. The shaded region is the associated standard error computed from the population variance. Note that the y scale is different for each LES case due to the range of N_d associated with each LES case.

In Figure 5, we generally observe that the domain-averaged $N_{d\_cal}^{3D}(\lambda_{abs})$ is underestimated compare to the domain-averaged $N_{d\_cal}^{1D}(\lambda_{abs})$ under high to moderate sun positions. However, this reverses towards more oblique SZAs, with the domain-averaged $N_{d\_cal}^{3D}(\lambda_{abs})$ becoming larger than $N_{d\_cal}^{1D}(\lambda_{abs})$ when the SZA increases towards larger values.

The physical impact of the 3D effects changes with the sun position: when the sun is high, absorption dominates horizontal transport differences between bands, but when the sun is low, horizontal transport is dominated by enhanced forward scattering across cloud boundaries. Thus our N_d result indicates that when the sun is high, horizontal transport is limited by absorption

https://doi.org/10.5194/egusphere-2025-4169
Preprint. Discussion started: 18 September 2025

leading to darkening effects in the SWIR that dominate in the $N_{d\_cal}^{3D}(\lambda_{abs})$ domain-averaged statistics, whereas brightening effects in the VNIR becomes dominant when the sun is oblique. The SZA at which the domain-averaged $N_{d\_cal}^{3D}(\lambda_{abs})$ overestimates its 1D counterpart varies with the different scene configuration and absorbing channel utilized for the bi-spectral retrieval. Interestingly, due to the strong absorption in the 3.7 μm band, in the ATEX polluted case (Figure 5i), the $N_{d\_cal}^{1D}(3.7\mu m)$ is always larger than the $N_{d\_cal}^{3D}(3.7\mu m)$ for all SZAs considered in this study.

3.3. N_d Derived at at Coarse Spatial Resolution

Because the relative amount of horizontal energy transport between pixels is reduced as the pixel size becomes larger, the behavior of 3D radiative effects is spatial resolution dependent. So far, this study has focused on retrievals at the native LES resolution (100 m). At these high spatial resolutions, retrievals are more sensitive to 3D radiative effects, including cloud vertical inhomogeneity, and microphysical assumptions (e.g., drizzle in the ATEX clean case). However, at the coarser spatial resolutions common in global satellite imager retrievals (e.g., MODIS, Visible Infrared Imaging Radiometer Suite (VIIRS)), the impact of horizontal cloud inhomogeneity on cloud retrievals can be complicated by PPHA biases, which are caused by inter-pixel horizontal heterogeneity (vs. sub-pixel heterogeneity), though the practical difference between the two effects is part of a continuum. Regardless, it is important to extend the analysis of the derived N_d to coarser satellite-scale resolutions.

We examine the behavior of N_d derived from a MODIS or VIIRS-like resolution (800 m is convenient for our LES models) using retrievals from area-averaged 3D RT simulated reflectances, and then compare those N_d PDFs with derived N_d obtained from 3D RT simulations at the native

https://doi.org/10.5194/egusphere-2025-4169
Preprint. Discussion started: 18 September 2025

LES resolution (100 m). The PDF comparison of $N_{d\_cal}^{3D}(2.1\mu m)$ obtained at both LES and coarse 800 m resolution when all cloudy pixels (i.e., partially cloudy and overcast cloudy pixels; refer to Sect. 2.3 for definition) are considered, is shown in Figure 6 and when only overcast cloudy pixels are considered is presented in Figure 7. From Figure 6, we clearly see that when all cloudy pixels are considered, the derived N_d PDF at the coarse 800 m resolution are distinct from those at the native LES resolution: the PDF of $N_{d\_cal}^{3D}(2.1\mu m)$ at the LES resolution is mostly skewed towards smaller N_d values, for the three solar geometries shown, with smaller in-cloud mean values for the coarse resolution compared to the corresponding LES resolution. The reason for this is due to the contribution of partially cloudy pixels in the coarse resolution retrievals, further enhancing the impact of the plane-parallel r_e bias contribution and result in smaller N_d values.

https://doi.org/10.5194/egusphere-2025-4169
Preprint. Discussion started: 18 September 2025

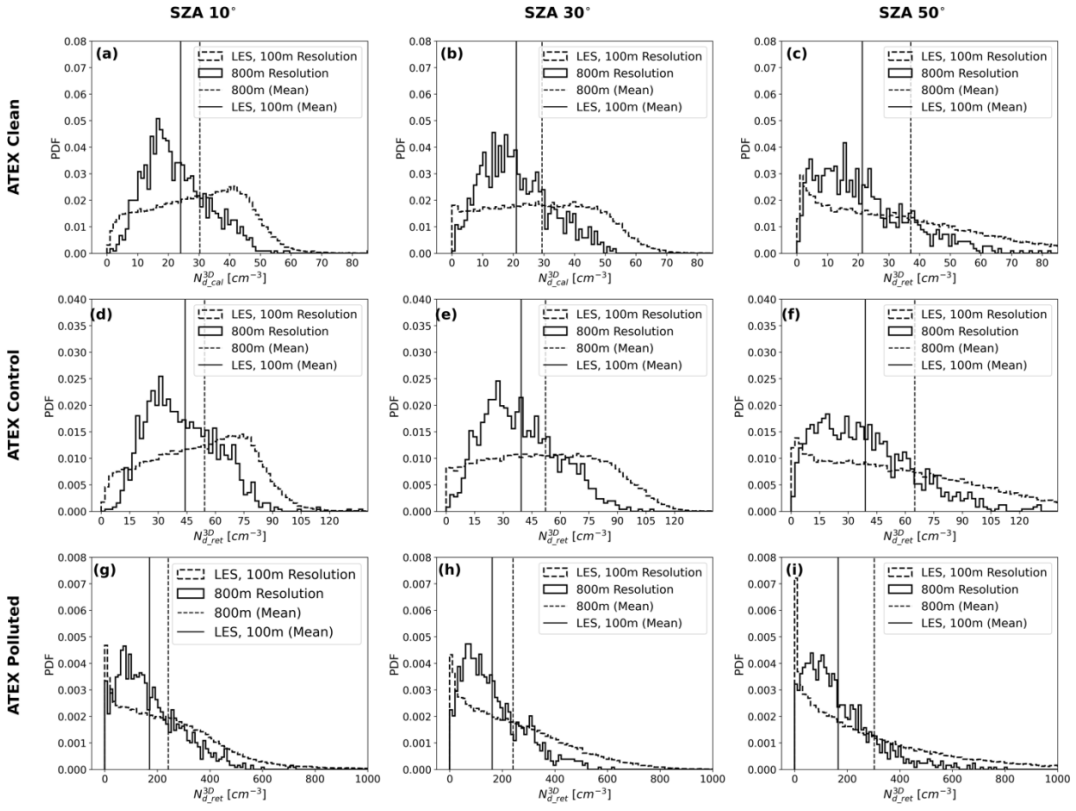

Figure 6. Probability Density Functions (PDFs) comparison of $N^{3D}_{d\_cal}(2.1\mu m)$ for LES (100 m) and coarse satellite-like (800 m) resolution for all cloudy pixels, at *SZA* 10^o, 30^o and 50^o for the ATEX clean, control and polluted case across all time steps. Vertical lines represent mean values.

https://doi.org/10.5194/egusphere-2025-4169
Preprint. Discussion started: 18 September 2025

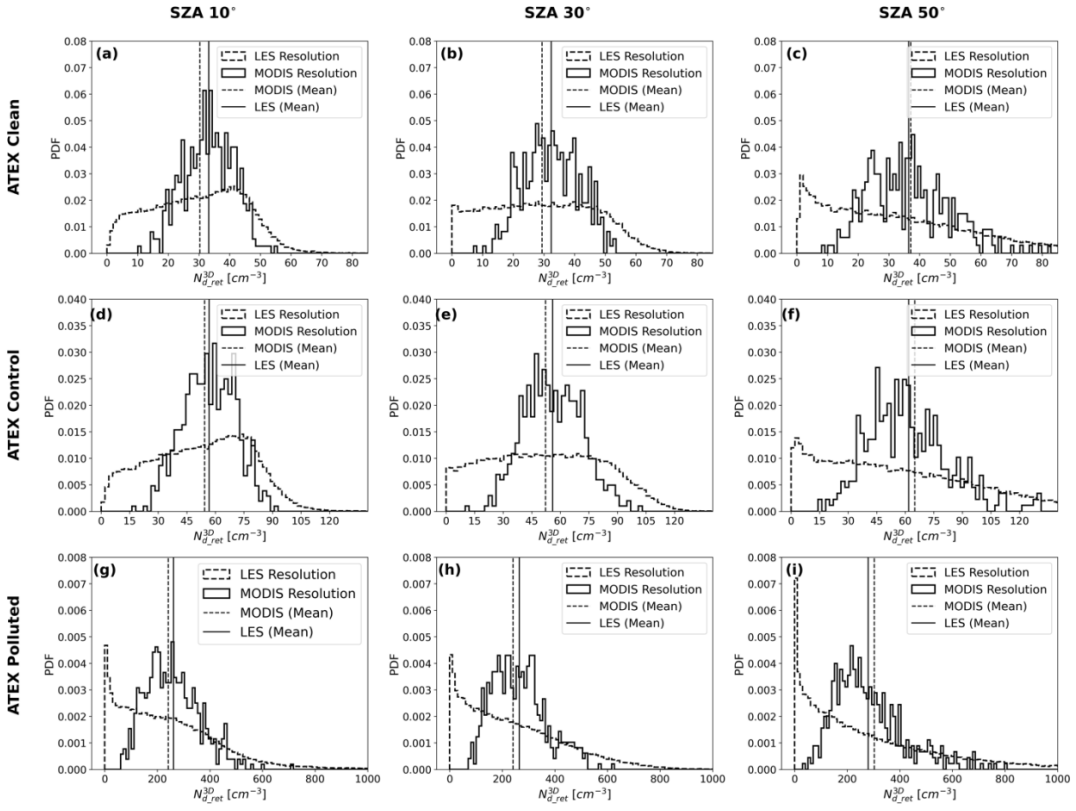

Figure 7. Probability Density Functions (PDFs) comparison of $N_{d\_cal}^{3D}(2.1\mu m)$ for LES (100 m) and coarse satellite-like (800 m) resolution for overcast cloudy only pixels, at SZA 10^o, 30^o and 50^o for the ATEX clean, control and polluted case across all time steps. Vertical lines represent mean values.

When only overcast cloudy pixels are considered (Figure 7), the contribution of the partially cloudy pixels is reduced and the smaller N_d values observed in Figure 6 are mostly absent. As seen in Figure 7, the PDFs of $N_{d\_cal}^{3D}(2.1\mu m)$ at the coarse (800 m) resolution, are mostly centered around moderate N_d values, and perhaps surprisingly, happen to have mean values that closely match corresponding values at the LES (100 m) resolution compared to results which utilize all cloudy pixels in the retrievals. These results can provide some additional confidence in using N_d calculations at coarse resolution for our LES cloud fields, as the effects of cloud heterogeneity

https://doi.org/10.5194/egusphere-2025-4169
Preprint. Discussion started: 18 September 2025

and opposing brightening and darkening 3D effects appear to cancel out (to a large extent) and still provide comparable mean values (although this depends on how well the satellite can identify partially cloudy pixels).

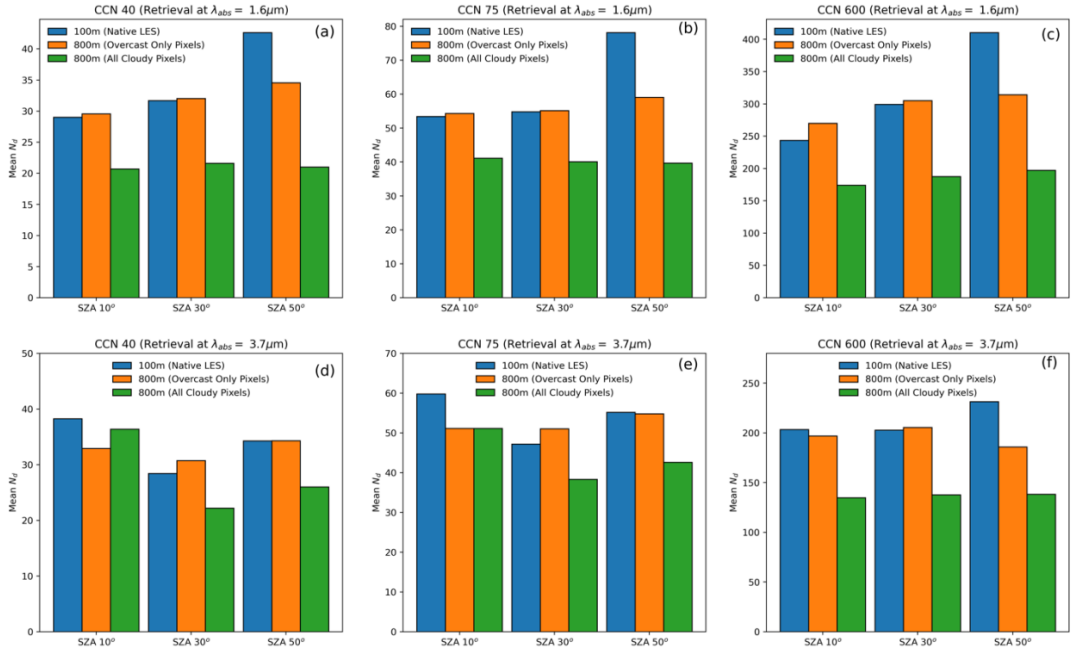

Figure 8. Comparison of mean $N_{d\_cal}^{3D}(\lambda_{abs})$ obtained at LES resolution of 100 m and coarse 800 m resolution for overcast cloudy only and all cloudy pixels, at SZA 10^o, 30^o and 50^o for the ATEX clean, control and polluted case across all time steps for λ_{abs} = 1.6 and 3.7 μm.

Mean values of $N_{d\_cal}^{3D}(\lambda_{abs})$ obtained at the native LES (100 m) and coarse satellite-like (800 m) resolution when λ_{abs} is 1.6 and 3.7 μm are presented in Figure 8. The results generally show that for λ_{abs} = 1.6 μm, the mean $N_{d\_cal}^{3D}$ at the LES native resolution, is more comparable to results from the coarse resolution, when considering only overcast cloudy pixels than to those obtained when all cloudy pixels are included (Figures 8 a, b and c). Results when λ_{abs} = 3.7 μm, also show that the mean $N_{d\_cal}^{3D}$ at the LES native resolution, is more comparable to results from the coarse

https://doi.org/10.5194/egusphere-2025-4169
Preprint. Discussion started: 18 September 2025

resolution, when considering only overcast cloudy pixels than to those obtained when all cloudy pixels are considered, except for the SZA 10° case, where results which utilize all cloudy pixels are slightly better than the overcast pixels only, but regardless, both are still comparable to the LES resolution result (Figures 8d, e and f).

3.4. Implications for Estimating Twomey Effect from Retrievals

Having investigated the impacts of 3D effects on the retrievals of τ and r_e, and the subsequently derived N_d, in this section we examine the consequent implications for estimating Twomey effect from these retrievals. In many previous studies, Twomey effect is usually estimated from observations using the so-called absolute cloud albedo susceptibility (S_{alb}) that connects the change of cloud albedo (α) with the change of N_d at a given LWP (Ackerman et al., 2000; Platnick and Twomey, 1994),

$$S_{alb} \equiv \frac{\partial \alpha}{\partial N_{d\_cal}}\Big|_{LWP} \approx \frac{\partial \alpha}{\partial \tau} \cdot \frac{\partial \tau}{\partial N_{d\_cal}}\Big|_{LWP}. \quad (6)$$

While S_{alb} is often derived empirically through numerical regression of satellite retrievals, many researchers try to develop theoretical expectations for these relationships. This involves using the chain rule of differentiation (Eq. (6)), where the first term—how cloud albedo depends on cloud properties (e.g., $\frac{\partial \alpha}{\partial \tau}$), is usually estimated from simplified radiative transfer models such as the two-stream approximation. The second term—how τ changes with respect to N_d at constant LWP ($\frac{\partial \tau}{\partial N_{d\_cal}}|_{LWP}$) is often derived from idealized cloud models assuming constant LWC or sub-adiabatic conditions. Of course, the change of N_d can also potentially lead to the change of LWP

https://doi.org/10.5194/egusphere-2025-4169
Preprint. Discussion started: 18 September 2025

known as cloud adjustment, but it is beyond the scope of this study. Here, we first examine the impacts of 3D effect on the estimation of $\frac{\partial \tau}{\partial N_{d\_cal}}|_{LWP}$, which we define as the retrieval sensitivity $s(\tau)$. Because a constant N_d is assumed, regardless of the cloud vertical profile assumptions, the relationship $\tau \propto N_d^{1/3} LWP^{5/6}$ holds (Ackerman et al., 2000; Platnick and Twomey, 1994), and implies that,

$$s(\tau) \equiv \frac{\partial In\tau}{\partial InN_{d\_cal}}|_{LWP} \approx \frac{1}{3}. \quad (7)$$

Constraining fixed LWP regimes is required to evaluate $s(\tau)$ and S_{alb}. Thus, we group LWP into eight bins ranges (B1 to B8) as given in Table 1 below. We will point it out explicitly in the analysis whether the LWP bin categorization is based on the 1D or 3D retrievals.

Bin Category	**B1**	**B2**	**B3**	**B4**	**B5**	**B6**	**B7**	**B8**
LWP range $[gm^{-2}]$	43.66 – 52.72	52.72 – 62.50	62.50 – 74.10	74.10 – 88.55	88.55 – 109.20	109.20 – 142.61	142.61 – 212.19	212.19 – Max(LWP)

Table 1. Liquid Water Path (LWP) bins used in this study. B1 to B8 are the bin number representation. Max(LWP) =3333.33, is maximum LWP value obtained from the retrievals (computed by utilizing Max allowable r_e (40 μm) and Max allowable τ (150) in Eq. (5)).

Describing retrieval sensitivity requires numerical regression of $\partial In\tau$ with ∂InN_d. As will be demonstrated in this section, 3D effects can influence the estimation of $s(\tau)$ though two main mechanisms:

https://doi.org/10.5194/egusphere-2025-4169
Preprint. Discussion started: 18 September 2025

- The errors in τ and N_{d_cal} retrievals caused by the 3D effects as shown in Sect. 3.2 and 3.3 can in turn lead to errors in the $\partial In\tau$-∂InN_{d_cal} regression. We refer to this as the "**retrieval error effect**".
- To obtain the theoretical $s(\tau) \approx \frac{1}{3}$, the $\partial In\tau$-∂InN_{d_cal} regression must be performed at constant LWP. Since LWP is also derived from retrievals in reality, it is subject to errors caused by 3D effects. These errors can cause mis-categorization of LWP bins in the regression analysis. We refer to this as the "**LWP categorization error"**.

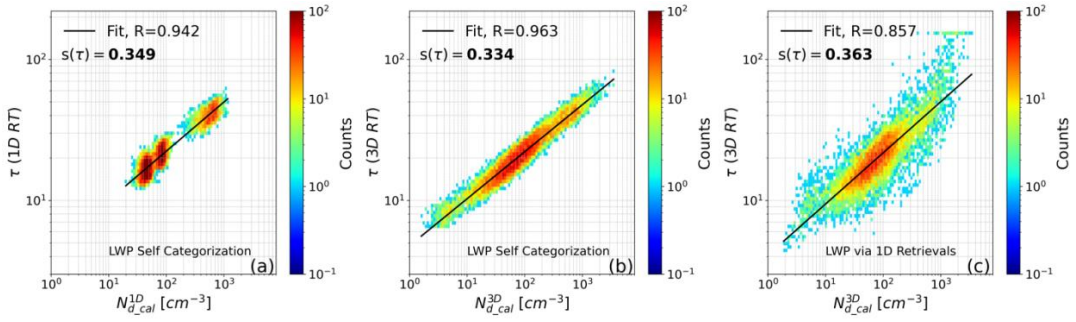

Figure 9. Regression plots of retrieved cloud optical thickness (τ) versus derived cloud droplet number concentration (N_d) for Liquid Water Path (LWP) bin 7 (B7; range 142.61 − 121.19 $g\ m^{-2}$), based on bi-spectral retrievals using the 0.86 µm and 2.1 µm channels at a large-eddy simulation (LES) resolution of 100 m and a solar zenith angle (SZA) of 50°. Panel (a) shows results under 1D radiative transfer (RT) using LWP bin categorization based on 1D retrievals (i.e., LWP Self-Categorization); panel (b) shows 3D RT results using LWP binning from 3D retrievals (i.e., LWP Self-Categorization); and panel (c) presents 3D RT results using LWP bin categorization based on 1D retrievals. Values in bold print indicate sensitivity $s(\tau)$ computed according to Eq. (7) and R is the correlation coefficient.

We first demonstrate the impact of retrieval and LWP categorization errors by calculating $s(\tau)$ from regressions of a single LWP bin (B7; 142.61 - 212.19 gm^{-2}). This analysis combines all three ATEX cases (clean CCN= 40 cm^{-3}, control CCN=75 cm^{-3}, and polluted CCN=600 cm^{-3}) utilizing the 0.86 µm and 2.1 µm channels at SZA 50°. The regressions shown in Figure 9 depict τ vs. N_{d_cal} and corresponding $s(\tau)$ obtained from regression. For both 1D and 3D retrievals based on LWP self-categorization (i.e., where LWP is determined consistently from cloud

https://doi.org/10.5194/egusphere-2025-4169
Preprint. Discussion started: 18 September 2025

properties retrieved from the respective RT reflectance fields), the regressions in Figure 9a and b clearly demonstrate a consistent power law scaling with different slopes; broadened variability in 3D retrievals, caused by 3D effects, which subsequently leads to a more consistent $s(\tau)$ value ($s(\tau) = 0.334$), even better than 1D RT result ($s(\tau) = 0.349$). However, in Figure 9c, we observe that clustering 3D retrievals into LWP bins using a reference dataset that is insensitive to the 3D radiative effects (in this case the reference LWP is calculated from 1D retrievals) leads to noticeably different distributions, where regression becomes less well correlated (correlation coefficient (R)= 0.857, compared to R > 0.9 for both LWP Self-categorization cases) and alters the calculated $s(\tau)$ value ($s(\tau)$ =0.363). This mismatch between retrievals and LWP classification highlights the importance of using a self-consistent LWP binning approach when calculating sensitivity. Maintaining consistency in LWP categorization is also important for accurately analyzing susceptibility estimates, as we will be shown later.

Having demonstrated the impact of 3D effects on $s(\tau)$ using a single representative LWP bin, we next use our simulations to investigate how these errors influence the cloud susceptibility. To evaluate this, it is useful to examine how albedo responds to variations in the relative droplet number concentration. Thus, we follow the approach of Painemal and Minnis (2012) and define relative albedo susceptibility ($S_{alb,rel}$), which accounts for the dependence of droplet number concentration on spatial variability, as:

$$S_{alb,rel} = N_{d\_cal}\frac{\partial \alpha}{\partial N_{d\_cal}}|_{LWP} = \frac{\partial \alpha}{\partial InN_{d\_cal}}|_{LWP}. \quad (8)$$

Analyzing $S_{\alpha,rel}$, which is based on fractional (logarithmic) changes in number concentration, will help to minimize the impact of absolute error biases in N_{d_cal} retrievals.

https://doi.org/10.5194/egusphere-2025-4169
Preprint. Discussion started: 18 September 2025

As stated in Sect. 2.2, since we are not directly simulating radiative fluxes and albedos in our RT solver, here (and in the remainder of this text), we would approximate,

$$S_{alb,rel} \propto \frac{\partial R_{BB}}{\partial InN_{d\_cal}}|_{LWP}. \quad (9)$$

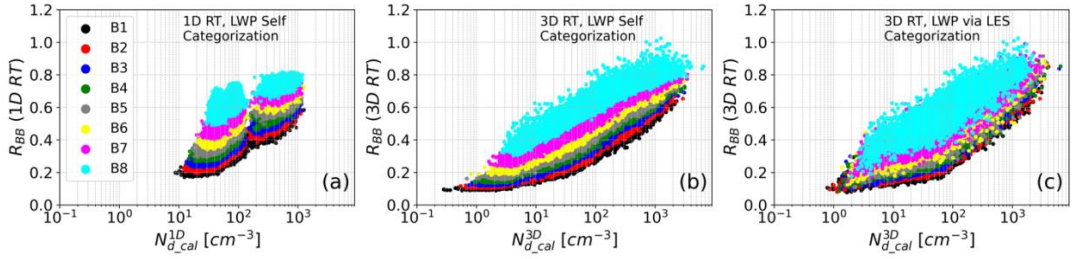

Figure 10. Scatter plots for similar liquid water path (LWP) bins showing R_{BB} vs. derived N_d (logarithmic scale) under 1D RT when LWP bin is categorized by 1D retrievals (LWP Self Categorization) in (a), under 3D RT when LWP bin is categorized by 3D retrievals (LWP Self Categorization) in (b), under 3D RT when LWP is categorized by LES LWP in (c). All carried out at SZA 50^o and bi-spectral retrievals pairing the 0.86 and 2.1μm channel at LES resolution of 100 m. (**LWP bins [g/m^2]- B1: 43.66 – 52.72, B2: 52.72 – 62.50, B3: 62.50 – 74.10, B4: 74.10 – 88.55, B5: 88.55 – 109.20, B6: 109.20 – 142.61, B7: 142.61 – 212.19, B8: 212.19 – 3333.33**).

The relationship between R_{BB} and N_{d_cal} for the eight LWP bins considered in this study (see Table 1) under 1D and 3D RT at SZA 50° at the LES native resolution (100 m) is presented in Figure 10. The scatter plots show R_{BB} versus N_{d_cal} estimates (calculated from the 0.86 and 2.1 μm bi-spectral retrieval) across all LES cases and time steps, under 3D and 1D RT using LWP self-categorization (Figure 10a and b) and LWP categorization based on LES model truth (Figure 10c). This Figure highlights a key feature of the first aerosol indirect effect (Twomey, 1977): an increase in droplet number concentration modifies cloud microphysics, leading to increases in both τ and albedo.

https://doi.org/10.5194/egusphere-2025-4169
Preprint. Discussion started: 18 September 2025

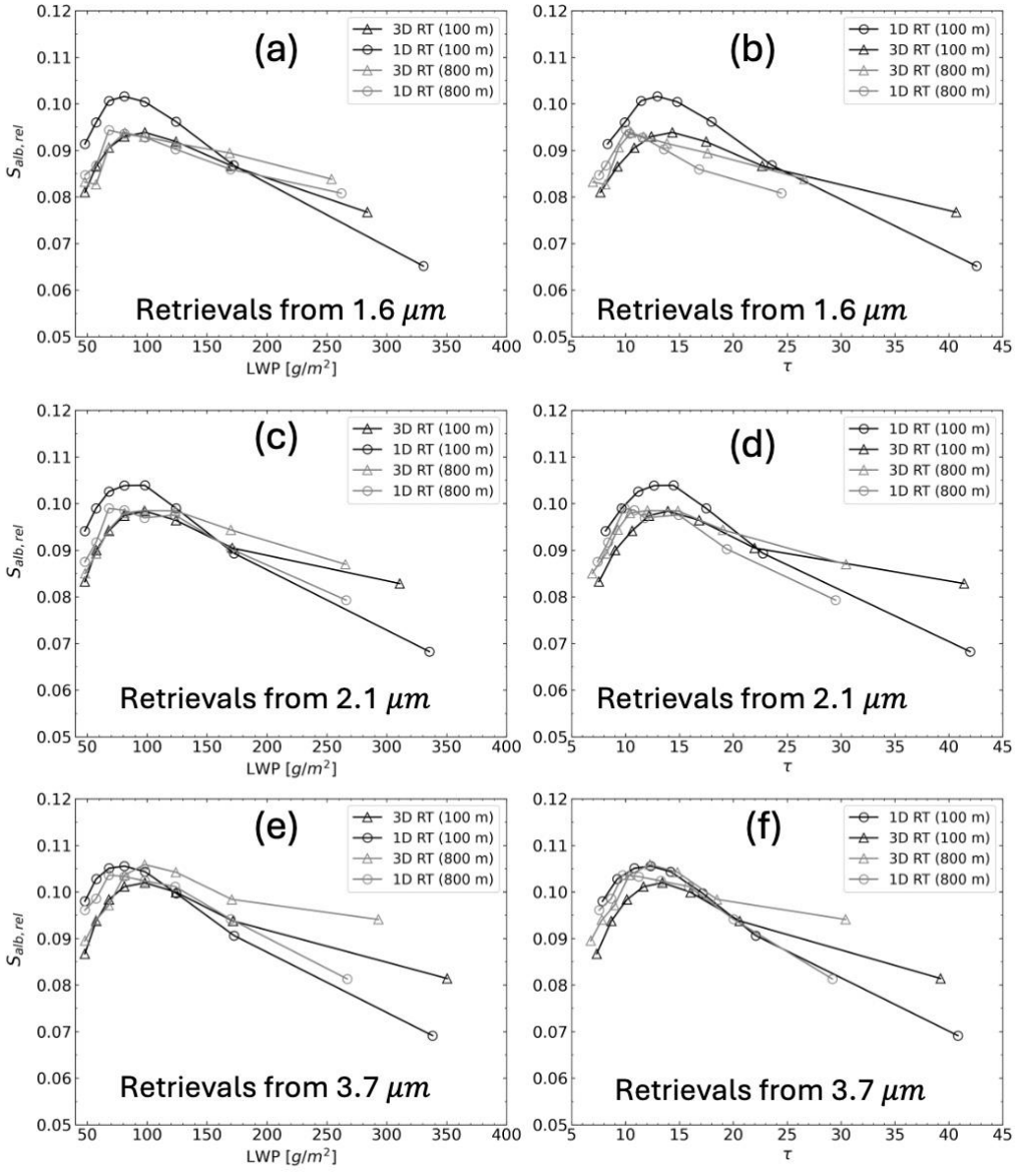

Figure 11. Mean relative cloud albedo susceptibility ($S_{alb,rel}$) across all six solar zenith angles (SZAs), shown as a function of liquid water path (LWP) in panels (a), (c), and (e), and as a function of cloud optical thickness (τ) in panels (b), (d) and (f). In each case, N_d and corresponding LWP or τ are retrieved by bi-spectral method using the reflectance pairs of 0.86 μm combined with 1.6 μm in (a) and (b), 2.1 μm in (c) and (d), and 3.7 μm in (e) and (f). Triangles represent $S_{alb,rel}$ derived from 3D RT results, while circles denote values from 1D RT. Gray solid lines indicate result of 800 m coarse resolution, and solid black lines represents LES-native resolution (100 m).

https://doi.org/10.5194/egusphere-2025-4169
Preprint. Discussion started: 18 September 2025

The R_{BB} vs. N_{d_cal} relationship under 3D RT for all LWP bins considered (B1 to B8; different colors in Figure 10b) spans a wider range of values, compared to its 1D counterpart (Figure 10a). The wide range of N_{d_cal} values in the 3D is due to the brightening and darkening 3D effects associated with the cloud property retrievals at oblique SZA (SZA 50°) which results in overestimation and underestimation of N_{d_cal}. As expected, categorizing the 3D RT results using LWP derived from the LES model—which is unaffected by 3D radiative effects—reveals a greater spread in each bin, suggesting LWP mismatch (Figure 10c) compared to 3D results with LWP self-categorization (Figure 10b). This underscores the importance of applying a consistent LWP categorization strategy when evaluating susceptibility estimate at fixed LWP. Subsequently, our relative susceptibility calculations will be all based on LWP self-categorization. The R_{BB}- N_{d_cal} relationship obtained when N_{d_cal} is derived from cloud properties retrieved by pairing the 0.86 μm with either the 1.6 or 3.7 μm band exhibits a similar pattern to that observed with the 0.86 and 2.1 μm combination (not shown).

To examine how 3D radiative effects impact our relative susceptibility calculations, we combine data across all LES cases (ATEX clean, control and polluted) and time steps for each corresponding R_{BB} and N_{d_cal} at the different SZA's (SZA= $[10^{\circ} : 60^{\circ}]$ in 10° intervals) in our study. Hereafter, the mean $S_{alb,rel}$ across all SZAs is calculated and the results analyzed. Figure 11 shows the mean $S_{alb,rel}$ computed under 3D and 1D RT as a function of mean LWP in each bin (Figure 11a, c and e) and mean $S_{alb,rel}$ as a function of mean τ in each LWP bin (Figure 11b, d and f) where cloud retrievals (r_e, τ) utilized to derive LWP and N_{d_cal} are retrieved from pairing the 0.86 μm channel with λ_{abs} of 1.6, 2.1 and 3.7 μm channel. At the native LES resolution, the plot shows that $S_{alb,rel}$ calculated from both 1D and 3D RT (for cloud retrievals from all three

https://doi.org/10.5194/egusphere-2025-4169
Preprint. Discussion started: 18 September 2025

absorbing bands) exhibits a similar pattern, characterized by an initial increase with LWP until it reaches a maximum (around $\tau \sim 13$, LWP $\sim 75 - 100\ gm^{-2}$), followed by a slight decrease, and then a more pronounced decrease at larger LWP / τ values.

When we compare $S_{alb,rel}$ results derived from 1D and 3D RT simulations. In the 1D case, R_{BB} is from 1D RT simulations, and N_{d_cal} is computed from τ and r_e retrieved using 1D reflectance. In the 3D case, R_{BB} is from 3D RT simulations, and N_{d_cal} is computed from τ and r_e retrieved using 3D reflectance. This comparison shows that for the three absorbing retrieval bands, the 3D results tend to underestimate its 1D counterpart at low to moderate LWP values, whereas the opposite is observed at higher LWP. This difference mostly disappears at coarse spatial resolution (gray symbols) as competition between plane parallel biases and 3D radiative effects apparently compensate one another. Because flux and these bi-spectral microphysical retrievals are radiatively traceable, the 1D and 3D results at coarse spatial resolution largely agree with one another in terms of radiative susceptibility. This indicates that at coarse spatial resolution, 3D effects and plane parallel biases in retrievals are compensating one another for relative radiative measures like $S_{alb,rel}$. Thus, concerns about pixel-level 3D effects retrieval biases at satellite resolution are unlikely to impact estimates of cloud radiative effects significantly. Retrieval artifacts can apparently bias our understanding of microphysical processes in clouds while not impacting our understanding of cloud radiative effects.

4. Summary and Conclusion

Errors associated with 3D radiative effects and cloud inhomogeneity can influence bi-spectral retrievals of cloud properties (τ and r_e), and subsequently impact estimates of N_d derived

https://doi.org/10.5194/egusphere-2025-4169
Preprint. Discussion started: 18 September 2025

from these properties. Because N_d is so important in the representation of clouds in models and the interpretation of aerosol–cloud effects, it is important to disentangle and explain these sources of retrieval bias. Therefore, this study focuses on investigating the impact of the 3D radiative effects on N_d calculated from τ and r_e retrieved by the bi-spectral method (N_{d_cal}) and further probes how an understanding of the first aerosol indirect effect is impacted when interpreted from such retrievals. We address this by a satellite observation-retrieval simulator framework, which consists of synthetic cloud fields, a radiative transfer solver and retrieval algorithm. The cloudy scenes examined here spanned numerous temporal snapshots from three LES cases, each of which was initialized based on observations made during the 1969 ATEX field campaign (NE Atlantic trade wind region ~12N, 35W). These LES cases are each characterized by different initial aerosol loadings: a clean (CCN = 40 cm^{-3}), control (CCN = 75 cm^{-3}), and polluted (CCN = 600 cm^{-3}) case. From these LES cloud fields, simulated reflectances (based on 1D and 3D RT) for MODIS Band 2 (0.86 μm), Band 6 (1.6 μm), Band 7 (2.1 μm), and Band 20 (3.7 μm) were carried out with the SHDOM RT model (Evans, 1998). Thereafter, bi-spectral retrievals were implemented on the simulated reflectance by pairing the 0.86 μm VNIR band with each of the absorbing wavelength bands (λ_{abs}= 1.6, 2.1 and 3.7 μm). Subsequently, N_{d_cal} were obtained from the bi-spectral microphysical retrievals at six solar geometries (SZA= [10° : 60°] in steps of 10°) and the results were analyzed.

We utilize N_d obtained from the LES as a reference and compare with N_{d_cal} derived from 1D RT simulations, and with N_{d_cal} inferred from the adiabatic assumption (Eq. (3)) when τ and r_e retrievals are constrained toward scenes that more closely approximate that assumption. Results demonstrates that, N_{d_cal} from τ and r_e retrieved from homogeneous plane parallel RT-based simulated reflectance can still be biased when compared to the reference N_d. This bias arises from

https://doi.org/10.5194/egusphere-2025-4169
Preprint. Discussion started: 18 September 2025

the complexity of how cloud microphysics is vertically distributed within realistic clouds, which may sometimes deviate from the adiabatic assumptions in which the N_{d_cal} equation is based. Also, the choice of the absorbing channel in the bi-spectral retrieval is a factor that contributes to this derived bias. Due to different liquid water absorption and therefore vertical sensitivities at different channels, the 3.7 μm band which has the strongest absorption, retrieves r_e closer to the cloud top, and agrees the most with the reference LES N_d, compared to results derived from pairing the 0.86 μm band with the 1.6 and 2.1 μm band.

To investigate how 3D radiative effects impact N_d estimates, we calculate N_{d_cal} using cloud properties derived from 1D RT-based reflectances and compare directly with N_{d_cal} calculated using cloud properties derived from 3D RT-based reflectances. These comparisons are performed for multiple bi-spectral band pairs (pairing VNIR= 0.86 μm with either of λ_{abs}= 1.6, 2.1, and 3.7). Results from this comparison carried out at different SZAs show that, for high sun (SZA=10°), the statistical distributions of $N_{d\_cal}(\lambda_{abs})$ from 3D and 1D RT agree well for all three LES cases. Domain-averaged $N^{3D}_{d\_cal}(\lambda_{abs})$ and $N^{1D}_{d\_cal}(\lambda_{abs})$ was also compared to determine the overall impact of the 3D (brightening and darkening) effects on the domain scale. For the high sun case, the domain-averaged $N^{3D}_{d\_cal}(\lambda_{abs})$ is underestimated compared to $N^{1D}_{d\_cal}(\lambda_{abs})$. This indicates that the darkening effect which dominates cloud property retrievals when the sun is high also dominates the domain-averaged $N^{3D}_{d\_cal}(\lambda_{abs})$ result (i.e., overestimated r_e and underestimated τ dominates the cloud property retrievals and yields lower $N^{3D}_{d\_cal}(\lambda_{abs})$ values compared to $N^{1D}_{d\_cal}(\lambda_{abs})$ results). A similar pattern is also observed for the domain-averaged $N^{3D}_{d\_cal}(\lambda_{abs})$ derived from not too oblique SZAs (e.g., SZA 30°).

https://doi.org/10.5194/egusphere-2025-4169
Preprint. Discussion started: 18 September 2025

When the sun is low at SZA 50°, the PDF distribution of $N_{d\_cal}^{3D}(\lambda_{abs})$ are more stretched and broad when compared to $N_{d\_cal}^{1D}(\lambda_{abs})$ results. A reason for this is that the cloud properties from which $N_{d\_cal}^{3D}(\lambda_{abs})$ is calculated, exhibits both underestimation and overestimation when compared to their 1D RT counterpart. This is expected since brightening and darkening 3D effects both occur in the 3D RT-simulated reflectance observation under low sun, which manifest in the cloud property retrieval as overestimation of τ and underestimation of r_e in brightened pixels and underestimation of τ and overestimation of r_e in darkened pixels. When we examine the domain-averaged results at low sun angles (typically SZA > 45°), the brightening effect appears to be dominant with domain-averaged $N_{d\_cal}^{3D}(\lambda_{abs})$ being overestimated compared to domain-averaged $N_{d\_cal}^{1D}(\lambda_{abs})$ as the SZA becomes large. Although, the exact SZA at which this overestimation occurs varies for the different λ_{abs} considered in this study.

The statistical distributions of N_{d_cal} at satellite-like (MODIS, VIIRS) pixel footprints were also examined. Compared to retrievals at the native LES resolution of 100 m, PDFs of $N_{d\_cal}^{3D}(2.1\mu m)$ derived at a resolution of 800 m exhibits some subtle differences depending on how one defines the cloud mask for the coarse resolution observations. We divide the retrieval population into two groups: all cloud retrievals (including partly cloudy) or overcast cloudy pixels (i.e., removing partly cloudy pixels). When all valid cloudy pixels are utilized for the averaging, the PDF of $N_{d\_cal}^{3D}(2.1\mu m)$ skews toward smaller N_{d_cal} values, indicating that the contribution of partially cloudy pixels, significantly impacts N_{d_cal} calculations. However, when only confident cloudy pixels are used, the PDF shifts away from these small N_{d_cal} values, and the mean N_{d_cal} at the LES and coarse satellite-like resolutions are comparable. Similar observations are also seen in the 1.6 and 3.75 μm derived N_d, where the mean N_{d_cal} at the LES and coarse

https://doi.org/10.5194/egusphere-2025-4169
Preprint. Discussion started: 18 September 2025

811 satellite-like resolutions are comparable, suggesting that retrievals from larger footprints can still
812 be reliable if only confident cloudy pixels are considered.

813 We show that the sensitivity $s(\tau)$, defined as the change in τ with respect to N_d at constant
814 LWP ($\frac{\partial \tau}{\partial N_{d\_cal}}|_{LWP}$), is influenced by both retrieval errors due to 3D radiative effects and LWP
815 categorization errors. The results reveal that 3D effects retrieval error cancel out in $s(\tau)$ calculated
816 under 3D RT using LWP self-categorization (i.e., LWP derived from r_e and τ retrieved from 3D
817 reflectance) to give $s(\tau)$ values that aligns closely to theoretical expectation (1/3), compared to
818 corresponding $s(\tau)$ values obtained when non-self-consistent LWP categorization is applied.

819 At the LES resolution, the average relative susceptibility ($S_{alb,rel}$) computed under 3D RT,
820 for retrievals computed from all three absorbing bands, underestimates the corresponding 1D RT
821 results at low LWP, and vice versa at larger LWP values. We further show that, at the coarse 800
822 m resolution, $S_{alb,rel}$, computed under 1D RT closely aligns with corresponding 3D RT results,
823 when evaluated as a function of average LWP and τ in each LWP bin across the six SZAs
824 considered in this study. This is due to cancellation of plane parallel bias and 3D effects errors to
825 give comparable results.

826 In conclusion, we demonstrate the impact of 3D effects on bi-spectral retrieval of τ and r_e
827 and their subsequent impact on the ability to infer N_d from such retrievals. While retrieval errors
828 can sometimes have far-reaching implications—biasing aerosol–cloud interaction studies that
829 attempt to constrain the impact of the first aerosol indirect effect (Quaas et al., 2020)—our study
830 shows that 3D effects have minimal impact on relative susceptibility at coarser satellite-like
831 footprints compared to results at fine LES resolution. Improvements in satellite retrievals of cloud
832 properties, from which N_d is inferred, remain important—especially the development of retrieval

https://doi.org/10.5194/egusphere-2025-4169
Preprint. Discussion started: 18 September 2025

methods that are less sensitive to 3D radiative effects. Recently, there has been increased development of polarimetric retrievals of cloud properties, offering the potential to constrain biases associated with r_e retrieval to the extent that the uppermost cloud layer microphysics captures the desired physics. However, the method of retrieving τ still utilizes the spectral technique, so any N_d retrieval derived from a polarimeter may not benefit from some of the compensating error impacts observed in this study for coarse-resolution observations. Other retrieval techniques such as cloud property retrievals using a combination of active and passive instruments (e.g., Sinclair et al., 2019) can also provide a better means to retrieve N_d and should be greatly encouraged.

Appendix A: N_d from the LES When Obtained as Column Average

For reference here we display our comparison of $N_{d\_cal}^{1D}(\lambda_{abs})$ vs. N_d from the LES cloud field, however this time we obtain the definition for the reference N_d from the in-cloud vertical column average N_d without weighting by β_{ext} as used in Eq. (1) (denoted as $\overline{N_{d\_LES}}$). Figure A1 shows these comparisons as a regression plot of $N_{d\_cal}^{1D}(\lambda_{abs})$ vs. $\overline{N_{d\_LES}}$ for the ATEX clean, control and polluted cases at 4.0 hours of simulation time, when λ_{abs} is 1.6, 2.1 and 3.7 μm. The comparison shows $N_{d\_cal}^{1D}(\lambda_{abs})$ mostly being overestimated compared to N_{d_LES} for the three LES cases. This is expected since $\overline{N_{d\_LES}}$ represents the central tendency and smaller values of N_d in the cloud column, particularly in regions close to the cloud top could directly impact the average value.

https://doi.org/10.5194/egusphere-2025-4169
Preprint. Discussion started: 18 September 2025

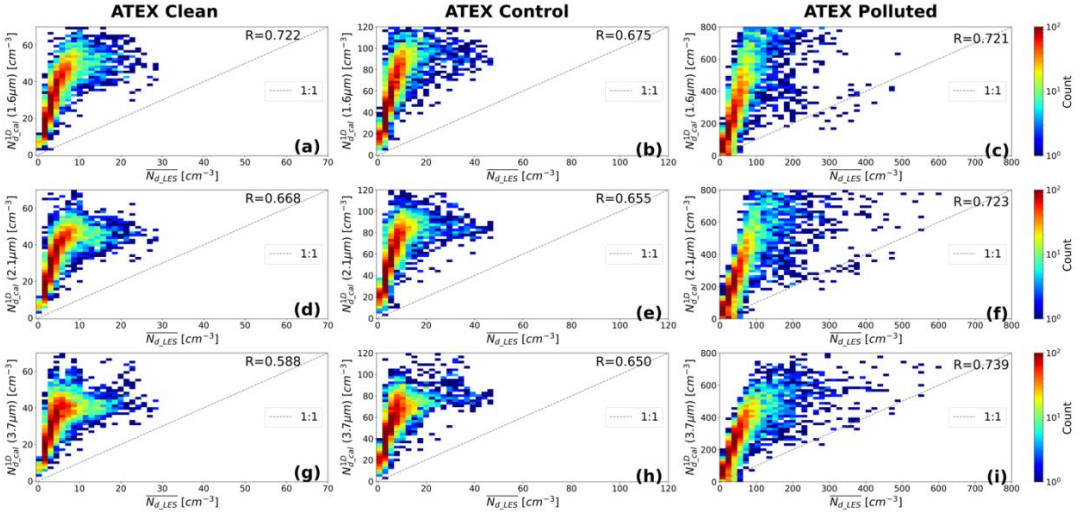

Figure A1. Comparison of N_d derived from 1D RT bi-spectral retrievals versus LES N_d obtained by vertical column average for (a) ATEX clean, (b) ATEX control and (c) ATEX polluted for retrievals at absorbing channel 1.6 μm, for (d) ATEX clean, (e) ATEX control and (f) ATEX polluted for retrievals at absorbing channel 2.1 μm and for (g) ATEX clean, (h) ATEX control and (i) ATEX polluted for retrievals at absorbing channel 3.7 μm at 4 h of simulation time. Note: 1D RT and bi-spectral retrievals utilized for this comparison were carried out at SZA 50°. Dotted lines indicate 1:1 relationship between the retrieved and LES N_d.

DATA AVAILABILITY The SHDOM radiative transfer code used in this study is freely available online from https://coloradolinux.com/shdom/ (SHDOM for Atmospheric Radiative Transfer is described in detail in a journal article available at https://doi.org/10.1175/1520-0469(1998)055<0429:TSHDOM>2.0.CO;2; Evans, 1998). The post-processed LES fields and radiative transfer simulation results for this study are available at https://doi.org/10.5281/zenodo.16945607 (Ademakinwa, 2025).

AUTHOR CONTRIBUTIONS Conceptualization, ZZ; methodology, ASA, ZZ and DM; software, ASA, DM; validation, ASA, DM and ZZ; formal analysis, ASA and DM; investigation, ASA and ZZ; data curation, ASA, ZZ; writing (original draft preparation), ASA; writing (review and editing), ASA, DM, JW, KGM, , SP, SP, ZHT, and ZZ; visualization, ASA; supervision, ZZ;

https://doi.org/10.5194/egusphere-2025-4169
Preprint. Discussion started: 18 September 2025

875 project administration, ZZ; funding acquisition, ZZ, JW, KGM, and SP. All authors have read and
876 agreed to the published version of the paper.

877

878 **ACKNOWLEDGMENTS** This study has been supported by the National Aeronautics and Space
879 Administration ACCESS project (grant no. 80NSSC21M0027). The hardware used in the
880 computational studies is part of the UMBC High Performance Computing Facility (HPCF). The
881 facility is supported by the U.S. National Science Foundation through the MRI program (grants
882 CNS-0821258 and CNS-1228778) and the SCREMS program (grant DMS-0821311), with
883 additional substantial support from the University of Maryland, Baltimore County (UMBC).

884 **Competing interests**: One of the authors is a member of the editorial board of ACP.

885

https://doi.org/10.5194/egusphere-2025-4169
Preprint. Discussion started: 18 September 2025

References

Ademakinwa, A. S., Zhang, Z., Miller, D., Meyer, K. G., Platnick, S., Tushar, Z. H., Purushotham, S., & Wang, J. (2025). Dataset for Manuscript: Impacts of the Three-dimensional Radiative Effects on Cloud Droplet Number Concentration Retrieval and Aerosol Cloud Interaction Analysis [Data set]. Zenodo. https://doi.org/10.5281/zenodo.16945607, 2025.

Ackerman, A. S., Hobbs, P. V., and Toon, O. B.: A Model for Particle Microphysics, Turbulent Mixing, and Radiative Transfer in the Stratocumulus-Topped Marine Boundary Layer and Comparisons with Measurements. *Journal of the Atmospheric Sciences*, *52*(8), 1204–1236. https://doi.org/10.1175/1520-0469(1995)052<1204:AMFPMT>2.0.CO;2 ,1995.

Ackerman, A. S., Kirkpatrick, M. P., Stevens, D. E., and Toon, O. B.: The impact of humidity above stratiform clouds on indirect aerosol climate forcing. *Nature*, *432*(7020), 1014–1017. https://doi.org/10.1038/nature03174, 2004.

Ackerman, A. S., Toon, O. B., Taylor, J. P., Johnson, D. W., Hobbs, P. V., and Ferek, R. J.: Effects of Aerosols on Cloud Albedo: Evaluation of Twomey's Parameterization of Cloud Susceptibility Using Measurements of Ship Tracks. *Journal of the Atmospheric Sciences*, *57*(16), 2684–2695. https://doi.org/10.1175/1520-0469(2000)057<2684:EOAOCA>2.0.CO;2, 2000.

Ademakinwa, A. S., Tushar, Z. H., Zheng, J., Wang, C., Purushotham, S., Wang, J., Meyer, K. G., Várnai, T., and Zhang, Z.: Influence of cloud retrieval errors due to three-dimensional radiative effects on calculations of broadband shortwave cloud radiative effect. *Atmospheric Chemistry and Physics*, *24*(5), 3093–3114. https://doi.org/10.5194/acp-24-3093-2024, 2024.

Albrecht, B. A.: Aerosols, Cloud Microphysics, and Fractional Cloudiness. *Science*, *245*(4923), 1227–1230. https://doi.org/10.1126/science.245.4923.1227, 1989.

https://doi.org/10.5194/egusphere-2025-4169
Preprint. Discussion started: 18 September 2025

909 Arola, A., Lipponen, A., Kolmonen, P., Virtanen, T. H., Bellouin, N., Grosvenor, D. P.,
910 Gryspeerdt, E., Quaas, J., and Kokkola, H.: Aerosol effects on clouds are concealed by natural
911 cloud heterogeneity and satellite retrieval errors. *Nature Communications*, *13*(1), 7357.
912 https://doi.org/10.1038/s41467-022-34948-5, 2022.
913 Bellouin, N., Quaas, J., Gryspeerdt, E., Kinne, S., Stier, P., Watson-Parris, D., Boucher, O.,
914 Carslaw, K. S., Christensen, M., Daniau, A. -L., Dufresne, J. -L., Feingold, G., Fiedler, S.,
915 Forster, P., Gettelman, A., Haywood, J. M., Lohmann, U., Malavelle, F., Mauritsen, T., …
916 Stevens, B.: Bounding Global Aerosol Radiative Forcing of Climate Change. *Reviews of*
917 *Geophysics*, *58*(1). https://doi.org/10.1029/2019RG000660, 2020.
918 Boers, R., Acarreta, J. R., and Gras, J. L.: Satellite monitoring of the first indirect aerosol effect:
919 Retrieval of the droplet concentration of water clouds. *Journal of Geophysical Research:*
920 *Atmospheres*, *111*(D22). https://doi.org/10.1029/2005JD006838, 2006.
921 Brenguier, J.-L., Burnet, F., and Geoffroy, O.: Cloud optical thickness and liquid water path – does
922 the andamp;lt;iandamp;gt;kandamp;lt;/iandamp;gt; coefficient vary with droplet
923 concentration? *Atmospheric Chemistry and Physics*, *11*(18), 9771–9786.
924 https://doi.org/10.5194/acp-11-9771-2011, 2011.
925 Cahalan, R. F., Ridgway, W., Wiscombe, W. J., Bell, T. L., and Snider, J. B.: The Albedo of
926 Fractal Stratocumulus Clouds. *Journal of the Atmospheric Sciences*, *51*(16), 2434–2455.
927 https://doi.org/10.1175/1520-0469(1994)051<2434:TAOFSC>2.0.CO;2, 1994.
928 Evans, K. F.: The Spherical Harmonics Discrete Ordinate Method for Three-Dimensional
929 Atmospheric Radiative Transfer. *Journal of the Atmospheric Sciences*, *55*(3), 429–446.
930 https://doi.org/10.1175/1520-0469(1998)055<0429:TSHDOM>2.0.CO;2, 1998. (code
931 available at: https://coloradolinux.com/shdom/, last access: 20 Janurary 2024).

https://doi.org/10.5194/egusphere-2025-4169
Preprint. Discussion started: 18 September 2025

Forster et al., , P., Storelvmo, T., Armour, K., Collins, W., Dufresne, J.-L., Frame, D., et al.: The Earth's Energy Budget, Climate Feedbacks and Climate Sensitivity. In *Climate Change 2021 – The Physical Science Basis* (pp. 923–1054). Cambridge University Press. https://doi.org/10.1017/9781009157896.009, 2021.

Fridlind, A. M., and Ackerman, A. S.: Estimating the Sensitivity of Radiative Impacts of Shallow, Broken Marine Clouds to Boundary Layer Aerosol Size Distribution Parameter Uncertainties for Evaluation of Satellite Retrieval Requirements. *Journal of Atmospheric and Oceanic Technology*, *28*(4), 530–538. https://doi.org/10.1175/2010JTECHA1520.1, 2011.

Grosvenor, D. P., Sourdeval, O., Zuidema, P., Ackerman, A., Alexandrov, M. D., Bennartz, R., Boers, R., Cairns, B., Chiu, J. C., Christensen, M., Deneke, H., Diamond, M., Feingold, G., Fridlind, A., Hünerbein, A., Knist, C., Kollias, P., Marshak, A., McCoy, D., … Quaas, J.: Remote Sensing of Droplet Number Concentration in Warm Clouds: A Review of the Current State of Knowledge and Perspectives. *Reviews of Geophysics*, *56*(2), 409–453. https://doi.org/10.1029/2017RG000593, 2018.

Gryspeerdt, E., Goren, T., Sourdeval, O., Quaas, J., Mülmenstädt, J., Dipu, S., Unglaub, C., Gettelman, A., and Christensen, M.: Constraining the aerosol influence on cloud liquid water path. *Atmospheric Chemistry and Physics*, *19*(8), 5331–5347. https://doi.org/10.5194/acp-19-5331-2019 , 2019.

Gryspeerdt, E., McCoy, D. T., Crosbie, E., Moore, R. H., Nott, G. J., Painemal, D., Small-Griswold, J., Sorooshian, A., and Ziemba, L.: The impact of sampling strategy on the cloud droplet number concentration estimated from satellite data. *Atmospheric Measurement Techniques*, *15*(12), 3875–3892. https://doi.org/10.5194/amt-15-3875-2022 , 2022.

https://doi.org/10.5194/egusphere-2025-4169
Preprint. Discussion started: 18 September 2025

954 Gryspeerdt, E., Quaas, J., and Bellouin, N.: Constraining the aerosol influence on cloud fraction.
955 *Journal of Geophysical Research: Atmospheres*, *121*(7), 3566–3583.
956 https://doi.org/10.1002/2015JD023744 , 2016.
957 Kato, S., and Marshak, A.: Solar zenith and viewing geometry-dependent errors in satellite
958 retrieved cloud optical thickness: Marine stratocumulus case. *Journal of Geophysical*
959 *Research: Atmospheres*, *114*(D1). https://doi.org/10.1029/2008JD010579 , 2009.
960 Loveridge, J. R., and Di Girolamo, L. (2024). Do Subsampling Strategies Reduce the Confounding
961 Effect of Errors in Bispectral Retrievals on Estimates of Aerosol Cloud Interactions? *Journal*
962 *of Geophysical Research: Atmospheres*, *129*(19). https://doi.org/10.1029/2023JD040189 ,
963 2024.
964 Marshak, A., Platnick, S., Várnai, T., Wen, G., and Cahalan, R. F.: Impact of three-dimensional
965 radiative effects on satellite retrievals of cloud droplet sizes. *Journal of Geophysical*
966 *Research: Atmospheres*, *111*(D9). https://doi.org/10.1029/2005JD006686 , 2006.
967 Martin, G. M., Johnson, D. W., and Spice, A.: The Measurement and Parameterization of Effective
968 Radius of Droplets in Warm Stratocumulus Clouds. *Journal of the Atmospheric Sciences*,
969 *51*(13), 1823–1842. https://doi.org/10.1175/1520-0469(1994)051<1823:TMAPOE>2.0.CO;2
970 , 1994.
971 McCoy, D. T., Bender, F. A. -M., Mohrmann, J. K. C., Hartmann, D. L., Wood, R., and Grosvenor,
972 D. P.: The global aerosol-cloud first indirect effect estimated using MODIS, MERRA, and
973 AeroCom. *Journal of Geophysical Research: Atmospheres*, *122*(3), 1779–1796.
974 https://doi.org/10.1002/2016JD026141 , 2017.

https://doi.org/10.5194/egusphere-2025-4169
Preprint. Discussion started: 18 September 2025

975 Meyer, K., Platnick, S., Arnold, G. T., Amarasinghe, N., Miller, D., Small-Griswold, J., Witte, M.,
976 Cairns, B., Gupta, S., McFarquhar, G., and O'Brien, J.: Evaluating spectral cloud effective
977 radius retrievals from the Enhanced MODIS Airborne Simulator (eMAS) during ORACLES.
978 *Atmospheric Measurement Techniques*, *18*(4), 981–1011. https://doi.org/10.5194/amt-18-
979 981-2025 , 2025.
980 Miller, D. J., Zhang, Z., Ackerman, A. S., Platnick, S., and Baum, B. A.: The impact of cloud
981 vertical profile on liquid water path retrieval based on the bispectral method: A theoretical
982 study based on large-eddy simulations of shallow marine boundary layer clouds. *Journal of*
983 *Geophysical Research: Atmospheres*, *121*(8), 4122–4141.
984 https://doi.org/10.1002/2015JD024322 , 2016.
985 Miller, D. J., Zhang, Z., Platnick, S., Ackerman, A. S., Werner, F., Cornet, C., and Knobelspiesse,
986 K.: Comparisons of bispectral and polarimetric retrievals of marine boundary layer cloud
987 microphysics: case studies using a LES–satellite retrieval simulator. *Atmospheric*
988 *Measurement Techniques*, *11*(6), 3689–3715. https://doi.org/10.5194/amt-11-3689-2018 ,
989 2018.
990 Nakajima, T. and King, M. D.: Determination of the Optical Thickness and Effective Particle
991 Radius of Clouds from Reflected Solar Radiation Measurements. Part I: Theory, J. Atmos.
992 Sci., 47, 1878–1893, https://doi.org/10.1175/1520-
993 0469(1990)047<1878:DOTOTA>2.0.CO;2, 1990.

https://doi.org/10.5194/egusphere-2025-4169
Preprint. Discussion started: 18 September 2025

Noone, K. J., Johnson, D. W., Taylor, J. P., Ferek, R. J., Garrett, T., Hobbs, P. V., Durkee, P. A., Nielsen, K., Öström, E., O'Dowd, C., Smith, M. H., Russell, L. M., Flagan, R. C., Seinfeld, J. H., De Bock, L., Van Grieken, R. E., Hudson, J. G., Brooks, I., Gasparovic, R. F., and Pockalny, R.: A Case Study of Ship Track Formation in a Polluted Marine Boundary Layer. *Journal of the Atmospheric Sciences*, *57*(16), 2748–2764. https://doi.org/10.1175/1520-0469(2000)057<2748:ACSOST>2.0.CO;2 , 2000.

Painemal, D., and Minnis, P.: On the dependence of albedo on cloud microphysics over marine stratocumulus clouds regimes determined from Clouds and the Earth's Radiant Energy System (CERES) data. *Journal of Geophysical Research: Atmospheres*, *117*(D6). https://doi.org/10.1029/2011JD017120 , 2012.

Platnick, S.: Vertical photon transport in cloud remote sensing problems. *Journal of Geophysical Research: Atmospheres*, *105*(D18), 22919–22935. https://doi.org/10.1029/2000JD900333 , 2000.

Platnick, S., and Oreopoulos, L.: Radiative susceptibility of cloudy atmospheres to droplet number perturbations: 1. Theoretical analysis and examples from MODIS. *Journal of Geophysical Research: Atmospheres*, *113*(D14). https://doi.org/10.1029/2007JD009654 , 2008.

Platnick, S., and Twomey, S.: Determining the Susceptibility of Cloud Albedo to Changes in Droplet Concentration with the Advanced Very High Resolution Radiometer. *Journal of Applied Meteorology*, *33*(3), 334–347. https://doi.org/10.1175/1520-0450(1994)033<0334:DTSOCA>2.0.CO;2 , 1994.

https://doi.org/10.5194/egusphere-2025-4169
Preprint. Discussion started: 18 September 2025

1014 Quaas, J., Arola, A., Cairns, B., Christensen, M., Deneke, H., Ekman, A. M. L., Feingold, G.,
1015 Fridlind, A., Gryspeerdt, E., Hasekamp, O., Li, Z., Lipponen, A., Ma, P.-L., Mülmenstädt, J.,
1016 Nenes, A., Penner, J. E., Rosenfeld, D., Schrödner, R., Sinclair, K., … Wendisch, M.:
1017 Constraining the Twomey effect from satellite observations: issues and perspectives.
1018 *Atmospheric Chemistry and Physics*, *20*(23), 15079–15099. https://doi.org/10.5194/acp-20-
1019 15079-2020 , 2020.
1020 Quaas, J., Boucher, O., and Lohmann, U.: Constraining the total aerosol indirect effect in the
1021 LMDZ and ECHAM4 GCMs using MODIS satellite data. *Atmospheric Chemistry and*
1022 *Physics*, *6*(4), 947–955. https://doi.org/10.5194/acp-6-947-2006 , 2006.
1023 Rajapakshe, C., and Zhang, Z.: Using polarimetric observations to detect and quantify the three-
1024 dimensional radiative transfer effects in passive satellite cloud property retrievals: Theoretical
1025 framework and feasibility study. *Journal of Quantitative Spectroscopy and Radiative*
1026 *Transfer*, *246*, 106920. https://doi.org/10.1016/j.jqsrt.2020.106920 , 2020.
1027 Sinclair, K., van Diedenhoven, B., Cairns, B., Alexandrov, M., Moore, R., Crosbie, E., and
1028 Ziemba, L.: Polarimetric retrievals of cloud droplet number concentrations. *Remote Sensing*
1029 *of Environment*, *228*, 227–240. https://doi.org/10.1016/j.rse.2019.04.008 , 2019.
1030 Stevens, B., Ackerman, A. S., Albrecht, B. A., Brown, A. R., Chlond, A., Cuxart, J., Duynkerke,
1031 P. G., Lewellen, D. C., Macvean, M. K., Neggers, R. A. J., Sánchez, E., Siebesma, A. P., and
1032 Stevens, D. E.: Simulations of Trade Wind Cumuli under a Strong Inversion. *Journal of the*
1033 *Atmospheric Sciences*, *58*(14), 1870–1891. https://doi.org/10.1175/1520-
1034 0469(2001)058<1870:SOTWCU>2.0.CO;2 , 2001.

https://doi.org/10.5194/egusphere-2025-4169
Preprint. Discussion started: 18 September 2025

1035 Stevens, D. E., Ackerman, A. S., and Bretherton, C. S.: Effects of Domain Size and Numerical
1036 Resolution on the Simulation of Shallow Cumulus Convection. *Journal of the Atmospheric*
1037 *Sciences*, *59*(23), 3285–3301. https://doi.org/10.1175/1520-
1038 0469(2002)059<3285:EODSAN>2.0.CO;2 , 2002.
1039 Twomey, S.: Pollution and the planetary albedo. *Atmospheric Environment (1967)*, *8*(12), 1251–
1040 1256. https://doi.org/10.1016/0004-6981(74)90004-3 , 1974.
1041 Twomey, S.: The Influence of Pollution on the Shortwave Albedo of Clouds. *Journal of the*
1042 *Atmospheric Sciences*, *34*(7), 1149–1152. https://doi.org/10.1175/1520-
1043 0469(1977)034<1149:TIOPOT>2.0.CO;2 , 1977.
1044 Twomey, S. and Cocks, T.: Remote Sensing of Cloud Parameters from Spectral Reflectance in the
1045 Near-Infrared, Beitr. Phys. Atmosph., 62, 172–179, 1989.
1046 Várnai, T., and Davies, R.: Effects of Cloud Heterogeneities on Shortwave Radiation: Comparison
1047 of Cloud-Top Variability and Internal Heterogeneity. *Journal of the Atmospheric Sciences*,
1048 *56*(24), 4206–4224. https://doi.org/10.1175/1520-0469(1999)056<4206:EOCHOS>2.0.CO;2
1049 , 1999.
1050 Várnai, T., and Marshak, A.: Observations of Three-Dimensional Radiative Effects that Influence
1051 MODIS Cloud Optical Thickness Retrievals. *Journal of the Atmospheric Sciences*, *59*(9),
1052 1607–1618. https://doi.org/10.1175/1520-0469(2002)059<1607:OOTDRE>2.0.CO;2 , 2002.
1053 Wood, R., and Hartmann, D. L.: Spatial Variability of Liquid Water Path in Marine Low Cloud:
1054 The Importance of Mesoscale Cellular Convection. *Journal of Climate*, *19*(9), 1748–1764.
1055 https://doi.org/10.1175/JCLI3702.1 , 2006.

https://doi.org/10.5194/egusphere-2025-4169
Preprint. Discussion started: 18 September 2025

1056 Zhang, Z., Ackerman, A. S., Feingold, G., Platnick, S., Pincus, R., and Xue, H.: Effects of cloud
1057 horizontal inhomogeneity and drizzle on remote sensing of cloud droplet effective radius:
1058 Case studies based on large-eddy simulations. *Journal of Geophysical Research:*
1059 *Atmospheres*, *117*(D19). https://doi.org/10.1029/2012JD017655 , 2012.
1060 Zhang, Z., Meyer, K., Yu, H., Platnick, S., Colarco, P., Liu, Z., and Oreopoulos, L.: Shortwave
1061 direct radiative effects of above-cloud aerosols over global oceans derived from 8 years of
1062 CALIOP and MODIS observations. *Atmospheric Chemistry and Physics*, *16*(5), 2877–2900.
1063 https://doi.org/10.5194/acp-16-2877-2016 , 2016.
1064 Zhang, Z., and Platnick, S.: An assessment of differences between cloud effective particle radius
1065 retrievals for marine water clouds from three MODIS spectral bands. *Journal of Geophysical*
1066 *Research Atmospheres*, *116*(20). https://doi.org/10.1029/2011JD016216 , 2011.
1067 Zhang, Z., Ackerman, A. S., Feingold, G., Platnick, S., Pincus, R., and Xue, H.: Effects of cloud
1068 horizontal inhomogeneity and drizzle on remote sensing of cloud droplet effective radius:
1069 Case studies based on large-eddy simulations, J. Geophys. Res.-Atmos., 117,
1070 D19208, https://doi.org/10.1029/2012JD017655, 2012.
1071 Zhu, Y., Rosenfeld, D., and Li, Z.: Under What Conditions Can We Trust Retrieved Cloud Drop
1072 Concentrations in Broken Marine Stratocumulus? *Journal of Geophysical Research:*
1073 *Atmospheres*, *123*(16), 8754–8767. https://doi.org/10.1029/2017JD028083 , 2018.
1074